The lncRNA *APOLO* interacts with the transcription factor WRKY42 to trigger root hair cell expansion in response to cold

Michaël Moison[*1], Javier Martínez Pacheco[*2], Leandro Lucero[*1], Camille Fonouni-Farde[1], Johan Rodríguez-Melo[3], Natanael Mansilla[1], Aurélie Christ[4], Jérémie Bazin[4]; Moussa Benhamed[4]; Fernando Ibañez[3], Martin Crespi[4], José M. Estevez[†,2,5] and Federico Ariel[†1]

[1] Instituto de Agrobiotecnología del Litoral, Universidad Nacional del Litoral, CONICET, FBCB/FHUC, Centro Científico Tecnológico CONICET Santa Fe, Colectora Ruta Nacional No 168 km. 0, Paraje El Pozo, Santa Fe 3000, Argentina.

[2] Fundación Instituto Leloir and IIBBA-CONICET, Av. Patricias Argentinas 435, Buenos Aires CP C1405BWE, Argentina.

[3] Instituto de Investigaciones Agrobiotecnológicas, CONICET, Universidad Nacional de Río Cuarto, Río Cuarto 5800, Argentina.

[4] Institute of Plant Sciences Paris-Saclay (IPS2), CNRS, INRA, University Paris-Saclay and University of Paris Bâtiment 630, 91192 Gif sur Yvette, France.

[5] Centro de Biotecnología Vegetal (CBV), Facultad de Ciencias de la Vida (FCsV), Universidad Andres Bello, Santiago, Chile and Millennium Institute for Integrative Biology (iBio), Santiago, Chile.

[*] These authors contributed equally to this work

[†] Correspondence to: Federico Ariel (fariel@santafe-conicet.gov.ar) and José M. Estevez (jestevez@leloir.org.ar)

Text Word count (without Abstract and References)**:** 6,287

ABSTRACT

Plant long noncoding RNAs (lncRNAs) have emerged as important regulators of chromatin dynamics, impacting on transcriptional programs leading to different developmental outputs. The lncRNA *AUXIN REGULATED PROMOTER LOOP* (*APOLO*) directly recognizes multiple independent loci across the *Arabidopsis* genome and modulates their three-dimensional chromatin conformation, leading to transcriptional shifts. Here, we show that *APOLO* recognizes the locus encoding the root hair (RH) master regulator ROOT HAIR DEFECTIVE 6 (RHD6) and controls *RHD6* transcriptional activity leading to cold-enhanced RH elongation. Furthermore, we demonstrate that *APOLO* interacts with the transcription factor WRKY42 and modulates its binding to the *RHD6* promoter. WRKY42 is required for the activation of *RHD6* by low temperatures and *WRKY42* deregulation impairs cold-induced RH expansion. Collectively, our results indicate that a novel ribonucleoprotein complex involving *APOLO* and WRKY42 forms a regulatory hub which activates *RHD6* by shaping its epigenetic environment and integrates signals governing RH growth and development.

Words: 148

Key words: root hairs; cell expansion; long noncoding RNAs; *APOLO*; transcription factors; RHD6; WRKY42; cold temperature

45 **INTRODUCTION**

46

47 Root hairs (RHs) are single cell projections developed from specialized epidermal trichoblast cells
48 able to increase their size several hundred times in a polar manner to reach and promote the uptake of
49 water-soluble nutrients, interact with soil microorganisms and support anchor to the plant. The specifi-
50 cation of epidermal cells into RHs is a complex process whose underlying mechanisms are partially un-
51 derstood. In *Arabidopsis thaliana*, RH cell fate is controlled by a developmental program involving a
52 complex of transcription factors (TFs) promoting the expression of the homeodomain protein GLABRA 2
53 (GL2) (Ryu et al., 2005; Song et al., 2011; Schiefelbein et al., 2014; Balcerowicz et al., 2015). GL2 blocks
54 RH development by inhibiting the transcription of the master regulator *ROOT HAIR DEFECTIVE 6* (*RHD6*)
55 (Lin et al., 2015). In the cells that differentiate into RHs (known as trichoblasts), a second TF complex
56 suppresses *GL2* expression (Schiefelbein et al., 2014), forcing the cells to enter the RH cell fate program
57 via the concomitant activation of RHD6 along with downstream TFs (Menand et al., 2007; Pires et al.,
58 2013). Briefly, RHD6 together with its homolog RSL1 (ROOT HAIR DEFECTIVE 6 LIKE 1) induce the expres-
59 sion of TFs from the bHLH family, including RSL2 (ROOT HAIR DEFECTIVE 6 LIKE 2) and RSL4 (ROOT HAIR
60 DEFECTIVE 6 LIKE 4), ultimately triggering the differentiation of the RHs and their subsequent polarized
61 tip-growth (Karas et al., 2009; Yi et al., 2010; Bruex et al., 2012). In addition, it was proposed that RSL4
62 controls the expression of a small subset of nearly 125 genes (Won et al., 2009; Yi et al., 2010; Datta et
63 al., 2015; Vijayakumar et al., 2016), including several cell wall extensins (EXTs) (Ringli, 2010; Velasquez et
64 al., 2011) sufficient to promote RH growth (Hwang et al., 2017).

65 RH expansion is regulated both by cell-intrinsic factors (e.g. endogenous phytohormones such as
66 auxin) and external environmental signals (e.g. phosphate (Pi) availability in the soil) (Mangano et al.,
67 2017; Bhosale et al., 2018). Pi starvation is one of the key environmental factors promoting rapid RH
68 growth (Yi et al., 2010; Datta et al., 2015; Vijayakumar et al., 2016). In *Arabidopsis*, it triggers *RSL4* ex-
69 pression via an enhanced auxin production, activating downstream effector genes mediating cell growth
70 (Yi et al., 2010; Datta et al., 2015; Mangano et al., 2017; Marzol et al., 2017; Bhosale et al., 2018). Ac-
71 cordingly, several auxin-related TFs have been implicated in Pi-starvation signaling in roots, including
72 WRKY proteins that control the expression of the Pi transporter families Pi-permease PHO1 and PHOS-
73 PHATE TRANSPORTER (PHT) (Devaiah et al., 2007; Chen et al., 2009; Wang et al., 2014; Su et al., 2015).
74 Under Pi-sufficient conditions, WRKY6 and WRKY42 bind to W-boxes of the *PHO1* promoter and suppress
75 its expression. During Pi starvation, WRKY42 is degraded by the 26S proteasome pathway, resulting in
76 the activation of *PHO1* transcription (Chen et al., 2009; Su et al., 2015). In addition, WRKY42 functions as

77 a positive regulator of *PHT1;1*, by binding to its promoter under Pi-sufficient condition (Su et al., 2015).
78 Overall, WRKY42 is part of the components activating root early-responses to Pi starvation, although its
79 role in controlling RH growth remains unexplored.

80 In recent years, plant long noncoding RNAs (lncRNAs) have emerged as important regulators of
81 gene expression, and several among them, have been functionally linked to Pi homeostasis. For instance,
82 the lncRNA *INDUCED BY PHOSPHATE STARVATION 1* (*IPS1*) can sequester the Pi starvation-induced mi-
83 croRNA miR-399, attenuating miR-399-mediated repression of *PHO2*, a gene encoding an E3 ligase af-
84 fecting Pi uptake (Franco-Zorrilla et al., 2007). In addition, the *cis*-natural antisense (*cis*-NAT) transcript
85 *PHO1;2*, induced under Pi deficiency, was shown to promote the translation of the *PHO1;2* mRNA in-
86 volved in Pi loading into the xylem. The expression of this *cis*-NAT is associated with the transport of the
87 sense–antisense RNA pair toward the polysomes (Jabnoune et al., 2013). More recently, it was shown
88 that the lncRNA *AUXIN REGULATED PROMOTER LOOP* (*APOLO*) recognizes multiple spatially independent
89 genes by sequence complementarity and DNA-RNA duplex formation, known as R-loops. Upon recogni-
90 tion, *APOLO* shapes the three-dimensional (3D) conformation of its target regions by decoying the
91 Polycomb Repressive Complex 1 (PRC1) component LIKE HETEROCHROMATIN PROTEIN 1 (LHP1), thereby
92 regulating their transcription (Ariel et al., 2014; Ariel et al., 2020).

93 Here, we show that the lncRNA *APOLO* directly regulates a subset of genes involved in RH devel-
94 opment, including the master regulator of RH initiation *RHD6*. *APOLO* activates *RHD6* transcription by
95 modulating the formation of a local chromatin loop encompassing its promoter region, an epigenetic
96 regulatory mechanism likely involving PRC1 and PRC2 components. Furthermore, we found that *APOLO*
97 interacts with the TF WRKY42, forming a new hub that regulates *RHD6* to induce RH growth in response
98 to low temperatures.

99

100 **RESULTS**

101

102 ***APOLO* regulates root hair cell elongation in response to low temperatures**

103 Based on Chromatin Isolation by RNA Purification (ChIRP-Seq) performed in wild-type (WT)
104 plants, it was previously reported that the lncRNA *APOLO* recognizes a subset of independent loci en-
105 riched in categories related to cell wall composition and organization (Ariel et al., 2020). A closer look at
106 *APOLO bona fide* targets allowed us to identify seventeen genes involved in RH growth and expansion
107 (**Supplementary Table 1**), a process dependent on cell wall remodeling molecules, including EXTs and
108 EXT-related proteins (Ringli, 2010; Lamport et al., 2011; Velasquez et al., 2011; Velasquez et al., 2015;

109 Marzol et al., 2018). Interestingly, according to single-cell RNA-seq datasets (Zhang et al., 2019) *APOLO*
110 transcripts are enriched in RH cells (**Supplementary Figure 1A**). Notably, sixteen *APOLO* direct targets
111 were upregulated upon *APOLO* over-expression (**Supplementary Table 2**). Furthermore, 52 additional RH-
112 related genes were upregulated in *35S:APOLO* seedlings (**Supplementary Table 2**) (Ariel et al., 2020).
113 Among them, the RH central TFs *RHD6* (as a direct target), *RSL2* and *RSL4* (as indirectly regulated) were
114 induced upon *APOLO* over-expression.

115 It was reported that the *APOLO* locus is targeted by the RNA-polymerase Pol V and silenced by
116 RNA-directed DNA Methylation (RdDM,(Ariel et al., 2014)). A search in a small RNA-Seq performed in WT
117 roots subjected to different temperature treatments (Gyula et al., 2018) revealed that RdDM-related 24nt
118 siRNA accumulation over the *APOLO* locus is less abundant at low temperatures (**Supplementary Figure**
119 **1B**), suggesting that *APOLO* transcription is regulated by cold. Accordingly, we found that *APOLO* tran-
120 scriptional accumulation increases in roots after 24h at 10°C (**Figure 1A**). An analysis of the promoter
121 activity of the 5.2kb region upstream *APOLO* (Ariel et al., 2020) directing the expression of a *GFP* reporter
122 gene, additionally revealed a higher transcriptional activity at low temperatures in the RHs (**Figure 1B**).
123 Strikingly, we observed that two RNAi-*APOLO* (repression of approximately 90%; Ariel et al., 2014) and
124 *35S:APOLO* independent lines (over expression of 30-fold and 60-fold, respectively; Ariel et al., 2020)
125 exhibit a basal increase of RH length at 22°C, and uncovered a strong induction of RH elongation in WT
126 and RNAi-*APOLO* at 10°C, in contrast to *35S:APOLO* lines (**Figure 1C**). Accordingly, *RHD6* is induced in re-
127 sponse to cold in WT roots, whereas RNAi-*APOLO* and *35S:APOLO* roots display higher *RHD6* basal levels
128 than the WT (**Figure 1D**). Notably, *RHD6* transcript levels are not further induced by cold in *35S:APOLO*
129 roots (**Figure 1D**), in agreement with the RH phenotype (**Figure 1C**). Collectively, our findings suggest that
130 *APOLO* participates in the induction of cold-mediated RH elongation and a deregulation of *APOLO* tran-
131 script levels can impact RH growth.

132 Previous studies pointed out a key role of RHD6 (together with RSL1) in RH development, which
133 is mediated by RSL4 and RSL2 as downstream regulators of RH cell elongation (Menand et al., 2007; Pires
134 et al., 2013). Notably, *RHD6*, *RSL2* and *RSL4* transcript levels were upregulated in *35S:APOLO* seedlings
135 (**Supplementary Table 2**; (Ariel et al., 2020)), although only *RHD6* was identified as a direct target of
136 *APOLO* (Ariel et al, 2020). In agreement with *RHD6* transcriptional behavior (**Figure 1D**), *RSL2* and *RSL4*
137 basal transcript levels are higher in RNAi-*APOLO* and *35S:APOLO* compared to WT. Interestingly, *RSL2*
138 and *RSL4* are induced by cold in WT and RNAi-*APOLO*, but not in *35S:APOLO* roots (**Supplementary Fig-**
139 **ure 2A**), suggesting that low temperatures can activate these two genes still in the absence of *APOLO*
140 and bypassing RHD6 for RH expansion (**Figure 1C**). Thus, we assessed if these TFs were also controlling

141 the promotion of RH growth by low temperatures. To this end, we tested how *rhd6/rsl1/rsl4* and *rsl2*,
142 *rsl4* and double mutant plants *rsl2/rsl4* respond to low temperatures in comparison with control condi-
143 tions **(Supplementary Figure 2A)**. The *rsl2* mutant was highly responsive to low temperatures in a similar
144 manner to WT while *rsl4* was impaired in the response to cold. The double mutant *rsl2/rsl4* and the triple
145 mutant *rhd6/rsl1/rsl4* did not develop RHs in either of the two conditions. In addition, constitutive ex-
146 pression of *RSL4* (*35S:RSL4*) as well as its expression under the control of the RH specific *EXPANSIN7*
147 promoter (*EXP7p:RSL4*) boosted basal RH growth without further enhancement in response to cold
148 (**Supplementary Figure 2B**). These results demonstrate that RSL4 is largely required for RHD6-dependent
149 activation of RH growth at low temperature, and RSL2 might participate to a lower extent.

150 Nutrient unavailability is known to activate RH expansion through a transcriptional reprogram-
151 ming governed by RHD6 and downstream TFs. The quantification of RH growth of WT plants in response
152 to increasing concentrations of nutrients (0.5X to 2.0X MS (Murashige and Skoog) medium) indicates that
153 high concentrations impair RH growth triggered by low temperatures **(Supplementary Figure 3A**). In a
154 similar way, an increase in agar concentration in the MS medium (from 0.8% to 2.5%), which likely re-
155 strains nutrient mobility (Singha, S., Townsend, E.C. and Oberly, 1985; Nonami and Boyer, 1989;
156 Ghashghaie et al., 1991; Buah et al., 1999) blocks cold-induced RH expansion **(Supplementary Figure 3B**).
157 Altogether, these observations suggest that low temperatures restrict nutrient mobility and availability in
158 the culture medium, leading to the promotion of polar RH growth.

159

160 ***APOLO* directly modulates the three-dimensional chromatin conformation of the root hair specific lo-**
161 **cus *RHD6***

162 Among *APOLO* targets involved in RH development, we found the master regulator of RH initia-
163 tion *RHD6* (Menand et al., 2007; Pires et al., 2013). The epigenetic profile of the *RHD6* locus corresponds
164 to typical *APOLO* targets (**Figure 2A**, (Ariel et al., 2020)), including H3K27me3 deposition (track 1), LHP1
165 recognition (track 2, chromatin immunoprecipitation (ChIP)-Seq, (Veluchamy et al., 2016)), and *APOLO*
166 binding regions (tracks 3 to 5, chromatin isolation by RNA purification (ChIRP)-Seq, (Ariel et al., 2020)). A
167 GAAGAA box, shown to be important for *APOLO* target recognition (Ariel et al., 2020) is located in the
168 *RHD6* locus and coincides with *APOLO* binding site. In addition, a peak of DNA-RNA hybrid
169 immunoprecipitation (DRIP)-Seq from root samples indicates the presence of an R-loop coinciding with
170 *APOLO* recognition sites over *RHD6* (tracks 6 to 8, (Xu et al., 2020)).

171 Remarkably, *APOLO* recognition and R-loop formation are also detectable over *RHD6* neighbor
172 gene, located 3.2 kb upstream *RHD6* transcription start site (**Figure 2A**). According to *Dpn*II Hi-C datasets

173 from Arabidopsis seedlings (Liu et al., 2016), a chromatin loop encompassing the intergenic region up-
174 stream *RHD6* was detected (**Figure 2B**), and coincides with *APOLO* binding-sites (**Figure 2A**, ChIRP-Seq).
175 By performing a ChIRP-qPCR with two independent sets of biotinylated probes to purify *APOLO* (ODD and
176 EVEN; (Ariel et al., 2020)) and one additional set used as a negative control (LacZ), we confirmed that
177 *APOLO* RNA–*RHD6* DNA interaction occurs in WT and is lost in *APOLO* knockdown (RNAi) seedlings ((Ariel
178 et al., 2014); **Figure 2C**). In addition, the quantification of relative *RHD6* loop formation in RNAi-*APOLO*
179 and *35S:APOLO* (Ariel et al., 2020) seedlings, revealed impaired loop formation in both lines (**Figure 2D**),
180 hinting at a stoichiometric requirement of *APOLO* for *RHD6* chromatin loop formation. Chromatin loop
181 formation (**Figure 2D**) is in agreement with *RHD6* basal levels in *35S:APOLO* and RNAi-*APOLO* lines (**Figure**
182 **1D**), suggesting that the chromatin loop including *RHD6* promoter region precludes transcription. Alto-
183 gether, our results indicate that *APOLO* lncRNA directly regulates *RHD6* transcriptional activity by fine-
184 tuning local chromatin 3D conformation.

185 It was previously reported that PRC2 actively participates in the regulation of RH growth (Ikeuchi
186 et al., 2015) and that the *RHD6* locus exhibits H3K27me3 deposition and LHP1 recognition (**Figure 2A;**
187 (Veluchamy et al., 2016)). Considering that the lncRNA *APOLO* interacts with the PRC1 component LHP1
188 *in vivo* (Ariel et al., 2014; Ariel et al., 2020), we decided to explore the role of PRC1 and PRC2 in *APOLO*-
189 mediated *RHD6* activation at low temperatures. At 22°C, *RHD6* suffers a reduction of H3K27me3 in the
190 PRC2 mutant *curly leaf* (*clf*), in contrast to the PRC1 mutant *lhp1* (**Supplementary Figure 4A;** (Veluchamy
191 et al., 2016)). Interestingly, we observed that H3K27me3 deposition and LHP1 binding diminish in WT
192 roots treated for 24h at 10°C compared to 22°C (**Supplementary Figure 4B**), consistent with the induction
193 of *RHD6* in response to cold (**Figure 2E**). Moreover, *lhp1* and *clf* mutants exhibit a basal decrease of RH
194 length together with a slight decrease of cold-induced RH elongation in *lhp1*, and a strong decrease of
195 cold-induced RH elongation in *clf* (**Supplementary Figure 4D**). Consistently, although the decrease in
196 H3K27me3 deposition results in higher basal transcript levels of *RHD6* in the *clf* background, *RHD6* tran-
197 scriptional activation by cold is abolished in the *clf* and *lhp1* mutants (**Supplementary Figure 4C**), hinting
198 at an important role of chromatin rearrangement for *RHD6* activation in response to cold.

199

200 ***APOLO* interacts with the transcription factor WRKY42 to coordinate the activation of *RHD6***

201 In order to uncover novel actors involved in cold-induced transcriptional regulation of RH
202 growth, we aimed at identifying *APOLO* protein partners. To this end, we performed an exploratory
203 ChIRP on WT seedlings using two independent set of biotinylated probes to purify *APOLO* (ODD and
204 EVEN; (Ariel et al., 2014; Ariel et al., 2020)), and one additional set used as a negative control (against

205 LacZ), as recently described (Rigo et al., 2020). Co-purified proteins were precipitated and analyzed by
206 mass spectrometry. Among the potential *APOLO* partners (i.e. identified with at least two hits in ODD
207 and EVEN samples, but absent in LacZ-ChIRP), we found the WRKY42 protein, a TF involved in the re-
208 sponse to Pi starvation (Su et al., 2015), an environmental condition that promotes RH cell expansion
209 (Bhosale, *et al.*, 2018) in a similar manner to low temperatures. Thus, *APOLO*-WRKY42 interaction was
210 validated by RNA immuno-precipitation (RIP-qPCR) in tobacco leaves and in *Arabidopsis* plants transitory
211 or stably transformed with 35S:*WRKY42:GFP*, respectively (**Figure 3A**). Interestingly, according to the
212 Arabidopsis eFP Browser (Waese et al., 2017), *WRKY42* is induced in roots when seedlings are subjected
213 to 4°C for 24h (**Figure 3B**). At 10°C, we observed that *WRKY42* transcriptional accumulation augments
214 significantly in roots (**Figure 3C**). Notably, 13 out of the 17 *APOLO* targets contained between 1 and 4
215 canonical WRKY TF binding sites (W-box) in their promoters, including *RHD6* (**Supplementary Table 1**).
216 By using a *35S:WRKY42:GFP* line, we determined that WRKY42 can directly bind to the promoter region
217 of *RHD6* (**Figure 3D**). Accordingly, the over-expression of *WRKY42* (*35S:WRKY42:GFP* line) led to a basal
218 increase of *RHD6* levels (**Figure 3E**) and RH elongation (**Figure 3F**) at ambient temperature, mimicking the
219 effect of cold. On the contrary, cold-mediated induction of *RHD6* is abolished in the *wrky42* mutant ((Su
220 et al., 2015); **Figure 3E**), which consistently exhibits shorter RHs at 22°C and almost no RH elongation at
221 low temperatures (**Figure 3F**). Taken together, these results suggest that the *APOLO*-interacting TF
222 WRKY42 is an important regulator of *RHD6*-mediated RH growth in response to cold.

223 We thus wondered to what extent WRKY42 regulates the epigenetic landscape of the *RHD6* lo-
224 cus. We first observed that H3K27me3 deposition over *RHD6* is significantly augmented in the *wrky42*
225 mutant background, in contrast to *AZG2*, an *APOLO* target non-related to WRKY42 (**Figure 4A**), con-
226 sistent with reduced *RHD6* basal levels reported in *wrky42* (**Figure 3E**). Therefore, we evaluated the mu-
227 tual contribution of *APOLO* and WRKY42 to their respective recognition of the *RHD6* locus. *APOLO* ChIRP-
228 qPCR in the WT and *wrky42* mutant (**Figure 4B**) revealed similar binding to *RHD6*, indicating that WRKY42
229 does not participate in *APOLO*-target recognition. Reciprocally, we assessed the control of *APOLO* over
230 WRKY42 recognition of the *RHD6* locus. To this end, we transformed transiently *A. thaliana* leaves of WT,
231 *35S:APOLO* and RNAi-*APOLO* plants with the construct *35S:WRKY42:GFP*. Observation using confocal
232 microscopy indicated that WRKY42:GFP is localized in the nucleus in the three genetic backgrounds
233 (**Supplementary Figure 5**). Remarkably, WRKY42:GFP ChIP-qPCR revealed that WRKY42 binding to *RHD6*
234 promoter is impaired both in *35S:APOLO* and RNAi-*APOLO* plants compared to WT (**Figure 4C**), hinting at
235 a stoichiometric role of *APOLO* in the modulation of TF-chromatin interaction. To further confirm our
236 observations, chromatin was extracted from *35S:WRKY42:GFP* seedlings and increasing amounts of *in*

237 *vitro* transcribed *APOLO* were added before cross-link and regular WRKY42 ChIP over *RHD6*. Strikingly,
238 increasing concentrations of *APOLO* gradually decoy WRKY42 away from the *RHD6* locus (**Figure 4D**),
239 further supporting the hypothesis of a stoichiometric regulation of *APOLO* over the activity of its partner
240 TF.

241 Collectively, our results indicate that the regulation of *RHD6* expression in response to cold
242 depends on Polycomb-dependent H3K27me3 dynamic deposition. The WRKY42-*APOLO* complex
243 modulates the epigenetic environment of *RHD6*, activating its transcription and promoting RH growth at
244 low temperatures. *RHD6* activation further triggers the expression of *RSL2* and *RSL4* that control the
245 transcriptional RH program inducing cell expansion in response to cold (**Figure 4E**).

246

247 **DISCUSSION**

248 Cell fate determination in the epidermis has been extensively studied (Ryu et al., 2005; Song et
249 al., 2011; Schiefelbein et al., 2014; Balcerowicz et al., 2015). Once trichoblast cells differentiate in the
250 root epidermis, RHs develop as fast polar growing protuberances in response to endogenous and envi-
251 ronmental signals (Menand et al., 2007; Yi et al., 2010; Pires et al., 2013; Marzol et al., 2017). RHs are
252 one of the main entry points in the roots for water-soluble macronutrients, such as Pi and nitrates. Pi is
253 an essential element for plant growth and development, and the availability of this macronutrient is a
254 factor limiting plant productivity. In Arabidopsis roots, low Pi in the soil triggers auxin synthesis and
255 transport, enhancing RH elongation to promote Pi uptake (Bhosale et al., 2018). Thus, auxin mediates
256 low Pi-induced promotion of RH cell expansion. Under low soil Pi, auxin synthesis is enhanced specifically
257 in the root cap (Stepanova et al., 2008) and transported (mostly by AUX1, PIN2, and PGP4) from the apex
258 to the differentiation zone, specifically leading to an increase of auxin levels in trichoblasts (Jones et al.,
259 2009; Bhosale et al., 2018; Wang et al., 2020). In response to the high-auxin microenvironment, RHs pro-
260 trude from the root epidermis controlled by RHD6 and RSL1(Menand et al., 2007; Pires et al., 2013). High
261 levels of auxin in trichoblasts trigger a signaling cascade mediated by TIR1-ARF19 (and possibly also
262 ARF7) which directly induces the expression of *RSL4* (and likely of *RSL2*) and promote RH elongation (Yi et
263 al., 2010; Mangano et al., 2017; Mangano et al., 2018b; Bhosale et al., 2018). ARF7 and ARF19 also acti-
264 vate other RH genes independently of RSL4 (Schoenaers et al., 2018). Interestingly, our results indicate
265 that the lncRNA *APOLO* participates in the response to low temperatures. *APOLO* is directly activated by
266 ARF7 and regulates the transcriptional activity of its neighboring gene *PINOID* (*PID*) by shaping local 3D
267 chromatin conformation (Ariel et al., 2014; Ariel et al., 2020). *PID* encodes a kinase responsible for accu-
268 rate auxin polar transport by localizing PIN2 in the root cell membrane (Friml et al., 2004). More recently,

269 it was shown that *APOLO* can recognize a subset of distant genes across the Arabidopsis genome, most
270 of them being related to auxin synthesis and signalling (Ariel et al., 2020). In this work, we demonstrate
271 that a group of RH related genes is directly regulated by *APOLO* in response to cold, including the RH
272 master regulator *RHD6*. Interestingly, *RSL2* and *RSL4* are still activated by cold in RNAi-*APOLO* roots in
273 contrast to *RHD6* (**Figure 1C** and **Supplementary Figure 2A**), suggesting that additional yet uncovered
274 factors, which might include ARF TFs, may trigger RH expansion in an *APOLO*/*RHD6*-independent man-
275 ner. Furthermore, we found that in addition to *RHD6*, *APOLO* directly regulates 16 RH-related genes
276 downstream *RHD6* and *RSLs* (**Supplementary Table 1**), hinting at an intricate regulatory network control-
277 ling RH expansion. Collectively, our results uncover a lncRNA-mediated epigenetic link between envi-
278 ronmental signals and auxin homeostasis modulating RH growth. Moreover, our observations suggest
279 that low temperatures restrict nutrient mobility and availability in the culture medium, leading to the
280 promotion of polar RH growth. Further research will be needed to determine what is the limiting nutri-
281 ent mediating the effect of cold on RH growth.

282 Although substantial progress has been achieved in the identification of the molecular actors
283 controlling RH development, the impact of chromatin conformation in the transcriptional regulation of
284 central TFs remains poorly understood. In this study, we have revealed a new mechanism of gene regula-
285 tion in RHs by which the lncRNA *APOLO* integrates chromatin-associated ribonucleoprotein complexes
286 together with the TF WYRK42, participating in the transcriptional activation of *RHD6* and the down-
287 stream RH gene network (**Figure 4D**). *APOLO* directly regulates the chromatin 3D conformation of the
288 genomic region encompassing the *RHD6* locus and stoichiometrically recruits WYRK42, previously linked
289 to Pi-starvation (Chen et al., 2009; Su et al., 2015). Low levels of *APOLO* fail to recruit WRKY42 to *RHD6*
290 promoter region, whereas high levels of *APOLO* likely decoy WRKY42 from target chromatin, as it was
291 shown for *APOLO* regulation over LHP1 binding activity (Ariel et al., 2020). Notably, low and high levels of
292 *APOLO* result in higher *RHD6* basal transcriptional accumulation (through LHP1 activity and change in
293 chromatin status), whereas both extremes impair *RHD6* activation by cold (through WRKY42 binding
294 modulation). Our results suggest that an WRKY42-*APOLO* hub regulates RH cell elongation through the
295 master regulator RHD6, although the *APOLO*-WYRKY42 hub potentially targets several additional cell wall
296 related genes (**Supplementary Table 1**) at the end of the pathway controlled by RHD6 and the RHD6-
297 downstream TFs RSL2/RSL4 (Mangano et al., 2017; Mangano et al., 2018a) .

298 Participation of epigenetic factors in root cell identity determination strongly suggests the de-
299 fault pattern for epidermal cell fate that can be overridden by environmental stimuli (Guimil and
300 Dunand, 2006). Interestingly, it was reported that the expression of *GLABRA2* (*GL2*), a gene encoding a

301 TF repressing *RHD6* in atrichoblasts, is tightly regulated at the epigenetic level. By using 3D fluorescence
302 *in situ* hybridization, it was shown that alternative states of chromatin organization around the *GL2* locus
303 are required to control position-dependent cell-type specification in the root epidermis (Costa and Shaw,
304 2006) . Furthermore, *GL2* epigenetic regulation was proposed to be responsive to salt stress (Beyrne et
305 al., 2019). In addition, a comprehensive characterization of alternative mutant lines uncovered the role
306 of PRC2 in the regulation of RH development (Ikeuchi et al., 2015). Loss-of-function mutants in different
307 PRC2 subunits develop unicellular RHs but fail to retain the differentiated state, generating a disor-
308 ganized cell mass from each single RH. It was shown that the resulting RHs are able to undergo a normal
309 endoreduplication program, increasing their nuclear ploidy, although they subsequently reinitiate mitotic
310 division and successive DNA replication. It was proposed that aberrant RH development in PRC2 related
311 mutants is due to the epigenetic deregulation of key regulatory genes such as *WOUND INDUCED DEDIF-*
312 *FERENTIATION 3* (*WIND3*) and *LEAFY COTYLEDON 2* (*LEC2*) (Ikeuchi et al., 2015). Here, we showed that
313 the single mutants *clf* (PRC2) and *lhp1* (PRC1) are affected in RH growth. In addition, we found that
314 H3K27me3 deposition and LHP1 binding to the *RHD6* locus is modulated by cold. Moreover, we showed
315 that in the *clf* background, H3K27me3 deposition throughout the *RHD6* locus is partially impaired, and
316 that the *clf* mutant is affected in RH elongation promoted by cold. Notably, basal transcriptional levels of
317 *RHD6* are higher in the *clf* mutant (Supplementary Figure 4C). A phenotypic characterization revealed
318 that RH density is not altered in *clf* or *lhp1* mutants, nor in *APOLO* and *WRK42* deregulated lines (**Sup-**
319 **plementary Figure 6**), suggesting that *RHD6* is not ectopically expressed in epidermic cells. Thus, *RHD6*
320 over-accumulation may occur in inner cell layers of the root or in RHs, although their elongation in the *clf*
321 mutant may be blocked by additional perturbations of Polycomb-associated regulation of downstream
322 genes. Altogether, our results suggest that Polycomb proteins participate in the control of RH-related
323 genes transcriptional reprogramming at low temperatures.

324 Notably, CLF and LHP1 were shown to interact with a subset of lncRNAs in *Arabidopsis*, modulat-
325 ing the activity of PRC target genes (Lucero et al., 2020). Interestingly, several lncRNAs have been linked
326 to the control of transcription in response to cold. *FLOWERING LOCUS C* is regulated by at least three
327 lncRNAs. First, the alternative splicing of a set of antisense transcripts, collectively named as *COOLAIR*,
328 depends on the prolonged exposure to cold, epigenetically repressing *FLC* (Marquardt et al., 2014). The
329 use of the *COOLAIR* proximal poly(A) site results in down-regulation of *FLC* expression in a process involv-
330 ing FLOWERING LOCUS D (FLD), an H3K4me2 demethylase (Marquardt et al., 2014). A second lncRNA
331 called *COLD ASSISTED INTRONIC NONCODING RNA* (*COLDAIR*) is fully encoded in the sense strand of the
332 first intron of *FLC.* Similar to *COOLAIR*, its accumulation oscillates in response to low temperatures. It was

333 proposed that *COLDAIR* recruits the PRC2 component CLF to target *FLC* for H3K27me3 deposition (Heo
334 and Sung, 2011). More recently, a third lncRNA modulating *FLC* transcription was identified (Kim and
335 Sung, 2017). The cold-responsive lncRNA *COLDWRAP* is derived from the *FLC* proximal promoter and it
336 also interacts with PRC2. It was suggested that *COLDWRAP* functions in cooperation with the lncRNA
337 *COLDAIR* to retain Polycomb at the *FLC* promoter through the formation of a repressive intragenic chro-
338 matin loop (Kim and Sung, 2017). Another lncRNA named *SVALKA* was shown to mediate the response to
339 low temperatures (Kindgren et al., 2018). Interestingly, the activation of *SVALKA* by cold triggers the
340 transcription of a cryptic downstream lncRNA, which overlaps the antisense locus of the *C-*
341 *repeat/dehydration-responsive element Binding Factor 1* (*CBF1*), involved in the early response to cold in
342 Arabidopsis. Antisense transcription causes Pol II head-to-head collision modulating transcriptional ter-
343 mination of *CBF1* (Kindgren et al., 2018). Here, we show that the auxin-responsive lncRNA *APOLO* is also
344 transcriptionally modulated by cold. The differential accumulation of 24nt siRNAs across the *APOLO* lo-
345 cus at low temperatures indicates that this activation is related to a decrease in RdDM. Moreover, we
346 showed here that the intergenic region between *PID* and *APOLO* acting as a divergent promoter is also
347 activated at low temperatures in RHs, as revealed by the reporter gene *GFP*. Thus, the lncRNA *APOLO*
348 integrates external signals into auxin-dependent developmental outputs in Arabidopsis.

349 In the last decade, lncRNAs have emerged as regulators of gene expression at different levels,
350 ranging from epigenetics to protein modifications and stability (Ariel et al., 2015). Notably, it has been
351 shown in animals that noncoding transcripts can be recognized by TFs. In humans, it was proposed that
352 the interaction with the lncRNA *SMALL NUCLEOLAR RNA HOST GENE 15* (*SNHG15*) stabilizes the TF Slug
353 in colon cancer cells. It was shown that *SNHG15* is recognized by the zinc finger domain of Slug prevent-
354 ing its ubiquitination and degradation in living cells (Jiang et al., 2018). Also, the transcriptional activity of
355 the human gene *DIHYDROFOLATE REDUCTASE* (*DHFR*) is regulated by a lncRNA encoded in its proximal
356 promoter. It was proposed that the nascent noncoding transcript forms a hybrid with its parent DNA and
357 decoys the regulatory TF IIB away from the *DHFR* promoter, dissociating the transcriptional pre-initiation
358 complex in quiescent cells (Martianov et al., 2007). The lncRNA *P21 ASSOCIATED ncRNA DNA DAMAGE*
359 *ACTIVATED* (*PANDA*) was identified in human cancer and it was activated in response to DNA damage
360 (Hung et al., 2011). *PANDA* is transcribed from the promoter region of the *CDKN1A* gene and interacts
361 with the TF NF-YA to limit the expression of pro-apoptotic genes. The activity of *PANDA* has been linked
362 to the progression of different tumors (Kotake et al., 2016; Shi et al., 2019). Interestingly, it was shown
363 that in addition to NF-YA, *PANDA* interacts with the scaffold-attachment-factor A (SAFA) as well as PRC1
364 and PRC2 to modulate cell senescence. In proliferating cells, SAFA and *PANDA* recruit Polycomb compo-

365 nents to repress the transcription of senescence-promoting genes. Conversely, the loss of SAFA–PANDA–
366 PRC interactions allows expression of the senescence program (Puvvula et al., 2014). In this work, we
367 showed that the PRC1-interacting lncRNA *APOLO* can also be recognized by the TF WRKY42, hinting at
368 general lncRNA-mediated mechanisms linking Polycomb complexes with the transcriptional machinery
369 across kingdoms. Furthermore, our observations indicate that the deregulation of *WRKY42* affects the
370 epigenetic environment of *RHD6*. It was previously shown that the addition of *in vitro* transcribed *APOLO*
371 to RNAi-*APOLO* chromatin extracts was able to partially restore R-loop formation over *APOLO* target
372 genes, and that high levels of *APOLO* may titer LHP1 away from chromatin (Ariel et al., 2020). Here we
373 show that the relative accumulation of the lncRNA *APOLO* can modulate the binding activity of its part-
374 ner TF to common target genes. Collectively, our results strongly support that environmentally con-
375 trolled cell fate in *Arabidopsis* relies on a transcriptional reprogramming governed by a network of epi-
376 genetic regulatory complexes, lncRNAs, TFs and effector proteins.
377
378 **MATERIALS AND METHODS**
379
380 **Plant Material and Growth Conditions.** All the *Arabidopsis thaliana* lines used were in the Columbia-0
381 (Col-0) background. *WRKY42* over expression transgenic plants were generated through *Agrobacterium*
382 *tumefaciens* (strain EHA105)-mediated transformation (Clough and Bent, 1998). *35S:WRKY42:GFP*
383 transformant lines were selected on MS/2 medium supplemented with kanamycin (40µg/mL) and
384 *WRKY42* expression levels were measured by RT-qPCR (primers used are listed in **Supplementary Table**
385 **3**). The *wrky42* mutant line belongs to the SALK collection (SALK_121674C), as the one previously charac-
386 terized (Su et al., 2015).The *rhd6-3/rsl1-1/rsl4-1*; *rsl2*; *rsl4*; *rsl2rsl4*, *35S:RSL4 and EXP7p:RSL4* transgenic
387 lines were previously described and characterized (Yi et al., 2010; Hwang et al., 2017) Homozygous
388 plants were obtained in our laboratory and genotyped using the oligonucleotides indicated in **Supple-**
389 **mentary Table 3**. Seeds were surface sterilized and stratified at 4°C for 2d before being grown under
390 long day conditions (16h light, 140µE.m^{-2}.sec^{-1}/8h dark), on ½-strength Murashige and Skoog media (1/2
391 MS) (Duchefa, Netherlands) with 0.8% plant agar (Duchefa, Netherlands).
392
393 **Cloning procedure.** The coding region of *WRKY42* (AT4G04450) excluding the STOP codon was amplified
394 by PCR, cloned into the Gateway entry vector pENTR/D-TOPO (Invitrogen) and recombined by Gateway
395 technology (LR reaction) into the pK7FWG2,0 vector containing a *p35S-GFP* cassette
396 (http://www.psb.ugent.be/gateway/index.php).

397

398 **Root hair phenotype characterization.** For quantitative analyses of RH phenotypes, 10 fully elongated
399 RH from the root elongation zone of 15-20 roots, were measured on the same conditions for each par-
400 ticular case and grown on vertical plates with ½-strength Murashige and Skoog media (1/2 MS) (Duchefa,
401 Netherlands) and 0.8% plant agar (Duchefa, Netherlands) for 5 days at 22° and 3 days at 10°C. Measure-
402 ments were made after 8 days. Images were captured with an Olympus SZX7 Zoom Stereo Microscope
403 (Olympus, Japan) equipped with a Q-Colors digital camera and software Q Capture Pro 7(Olympus, Ja-
404 pan). RH density was determined as the number of hairs in a representative area of the root elongation
405 zone using the same setup stated above and ImageJ software. Results were expressed as the mean ±
406 standard error (SE) and in the case of RH density, values were expressed per mm^2. All measurements
407 indicate the average of three independent experiments, each involving 15-20 seedlings.

408

409 **Confocal microscopy analysis of root hairs.** Confocal laser scanning microscopy was performed using
410 Zeiss LSM5 Pascal (Zeiss, Germany) and a 40x water-immersion objective, N/A=1.2. Fluorescence was
411 analyzed by using 488 nm laser for GFP excitation (Laser Intensity: 70%, Detector Gain:550, Amplifier
412 Offset:0.1, Amplifier Gain:1), and emitted fluorescence was recorded between 490 and 525nm for GFP
413 tag. Z stacks were done with an optical slice of 1µm, and fluorescence intensity was measured in 15µm
414 ROI (Region Of Interest) at the RH tip and summed for quantification of fluorescence using ImageJ. Five
415 replicates for each of ten roots and 15 hairs per root were observed. Col-0 wild type root hairs were used
416 as a negative control, to check autofluorescence signal occurrence and no signal were detected in the
417 wavelengths range stated above.

418

419 **RNA extraction and RT-qPCR.** Total RNA was extracted using TRIZol (Invitrogen) and 2 µg were subjected
420 to DNase treatment according to the manufacturer's protocol (Thermo Scientific). One µg of DNase-free
421 RNA was reverse-transcribed using Maxima H Minus Reverse Transcriptase (Thermo Scientific). RT-qPCR
422 were performed using the LightCycler 480 SYBR Green I Master Kit on a LightCycler480 apparatus
423 (Roche) using standard protocols (40 cycles, 60°C annealing). *PP2A* (AT1G13320; primers are listed in
424 **Supplementary Table 3**) was used as reference.

425

426 **RNA Immunoprecipitation.** RNA immunoprecipitation (RIP) assays were performed on transiently trans-
427 formed *N. benthamiana* leaves as described in (Sorenson and Bailey-Serres, 2015), or in 10-day-old *A.*
428 *thaliana 35S:WRKY42:GFP* seedlings as described in (Bardou et al., 2014), using anti GFP (Abcam ab290)

429 and anti-IgG (Abcam ab6702). RIP was performed using Invitrogen Protein A Dynabeads. Precipitated
430 RNAs were prepared using TRI Reagent (Sigma-Aldrich), treated with DNase (Fermentas) and subjected
431 to RT-qPCR (High Capacity cDNA Reverse Transcription Kit (Thermo); primers used are listed in **Supple-**
432 **mentary Table 3**). Total RNAs were processed in parallel and considered the input sample.
433
434 **Chromatin Immunoprecipitation.** Chromatin immunoprecipitation (ChIP) assays were performed on 10-
435 day-old WT seedlings treated or not during 24h at 10 °C, using anti H3K27me3 (Diagenode pAb-195-050),
436 anti LHP1 (Covalab pab0923-P) and anti-IgG (Abcam ab6702), as described in (Ariel et al., 2020).
437 Crosslinked chromatin was sonicated using a water bath Bioruptor Pico (Diagenode; 30sec ON/30sec OFF
438 pulses; 10 cycles; high intensity). ChIP was performed using Invitrogen Protein A Dynabeads. Precipitated
439 DNA was recovered using Phenol:Chloroform:Isoamilic Acid (25:24:1; Sigma) and subjected to RT-qPCR
440 (primers used are listed in **Supplementary Table 3**). Untreated sonicated chromatin was processed in
441 parallel and considered the input sample. For *in vitro* competition assays, *APOLO* was transcribed using
442 the T7 transcription kit (Promega; (Ariel et al., 2020)). After regular chromatin isolation from 10-day-old
443 *35S:WRKY42:GFP* seedlings, the sample was split in 4 independent tubes and diluted to 1ml in Nuclei
444 Lysis Buffer without SDS. 0 µg, 0.1 µg, 1 µg and 10 µg of *APOLO* were added to each sample respectively,
445 and incubated in rotation at 4 °C for 3h. Then, cross-linking was performed with 1% formaldehyde for 5
446 min at 4 °C, followed by 5 min with a final concentration of 50 mM glycine. SDS was added to a final con-
447 centration of 0.1% prior to sonication and the subsequent steps of a regular ChIP protocol.
448 For ChIP in transiently transformed leaves, 3-week-old *A. thaliana* were transformed as previously de-
449 scribed (Zhang et al., 2020) In brief, *Agrobacterium tumefaciens* strain GV3101 carrying *35S:WRKY42:GFP*
450 construct were grown for 2 days in YEB-induced medium plates at 28 °C. Agrobacterium cells were
451 scraped and resuspended in washing solution (10 mM $MgCl_2$, 100 µM acetosyringone). Infiltration solu-
452 tion (¼MS [pH = 6.0], 1% sucrose, 100 µM acetosyringone, 0.005% [v/v, 50 µl/l] Silwet L-77) was pre-
453 pared with the previous solution, adjusting the OD600=0.5. The infiltration was carried out in all leaves >
454 0.5cm in length of between 10 and 15 plants per genotype (WT, *35S:APOLO* and RNAi-*APOLO* lines). After
455 infiltration, plants were kept in light for 1h and then in darkness for 24h. Finally they were transferred
456 back to light. Images and samples were obtained 3 days after infiltration. For image acquisition, infiltrat-
457 ed leaves were imaged with a Leica TCS SP8 confocal laser scanning microscope with excitation at 488
458 nm (Intensity=8%) and detection at 495-530 nm for GFP and 610-670 (gain 650) nm for chlorophyll fluo-
459 rescence. Images were captured using 10X and 20X lenses, and processed using Fiji software (Schindelin
460 et al., 2012).

461

462 **Chromatin Isolation by RNA Purification followed by qPCR or mass spectrometry.** A method adapted
463 from the ChIRP protocol (Chu et al., 2012) was developed to allow the identification of plant DNA associ-
464 ated to specific lncRNAs, as described in (Ariel et al., 2014; Ariel et al., 2020). Briefly, plants were *in vivo*
465 crosslinked and cell nuclei were purified and extracted through sonication. The resulting supernatant
466 was hybridized against biotinylated complementary oligonucleotides that tile the lncRNA of interest and
467 lncRNA-associated chromatin was isolated using magnetic streptavidin beads. One hundred pmol of
468 probes against *APOLO* (ODD and EVEN set of probes (Ariel et al., 2014; Ariel et al., 2020)) and the corre-
469 sponding negative set against LacZ were used for independent purification. Co-purified
470 ribonucleoprotein complexes were eluted and used to purify RNA or DNA, which were later subjected to
471 downstream assays for quantification as previously described (Ariel et al., 2020).
472 The exploratory identification of plant nuclear proteins bound to *APOLO* was performed as described in
473 (Rigo et al., 2020). Plant samples were prepared as for ChIRP-qPCR. For protein extraction, approximately
474 250 g of 7-day-old Col-0 plants grown on solid half-strength MS medium was irradiated three times with
475 UV using a CROSSLINKERCL-508 (Uvitec) at 0.400 J/ cm^2. Protein purification samples for protein extrac-
476 tion were DNase-treated according to the manufacturer (Thermo Scientific). After addition of 1.8ml of
477 TCA-acetone (5ml 6.1N TCA + 45ml acetone + 35µl β-mercaptoethanol), samples were incubated over-
478 night at -80°C. After centrifugation at 20000rpm for 20min at 4°C, the supernatant was discarded and
479 1.8ml of acetone wash buffer (120ml acetone, 84µl β-mercaptoethanol) was added to the samples.
480 Then, samples were incubated 1h at -20°C and centrifuged again at 20000 rpm for 20min at 4°C. The
481 supernatant was discarded, and the dry pellet was used for mass spectrometry analyses.
482

483 **Chromatin Conformation Capture.** Chromosome conformation capture (3C) was performed basically as
484 previously described in (Ariel et al., 2020) starting with 2g of seedlings. Digestions were performed over-
485 night at 37°C with 400U *Dpn*II (NEB). DNA was ligated by incubation at 16°C for 5h in 4 ml volume using
486 100U of T4 DNA ligase (NEB). After reverse crosslinking and Proteinase K treatment (Invitrogen), DNA
487 was recovered by Phenol:Chloroform:Isoamilic Acid (25:24:1; Sigma) extraction and ethanol precipita-
488 tion. Relative interaction frequency was calculated by qPCR (primers used are listed in **Supplementary**
489 **Table 3**). A region free of *Dpn*II was used to normalize the amount of DNA.
490

491 **Acknowledgments**

492 We thank Chang Liu for providing the Hi-C plot of Figure 2B. This work was supported by grants from
493 ANPCyT (PICT2016-0132 and PICT2017-0066) and Instituto Milenio iBio – Iniciativa Científica Milenio,
494 MINECON to JME; ANPCyT (PICT2016-0007 and PICT2016-0289) and Fima Leloir Award to FA; UNL (CAI+D
495 2016) to LL; Laboratoire d'Excellence (LABEX) Saclay Plant Sciences (SPS; ANR-10-LABX-40) to MC; and
496 CNRS (Laboratoire International Associé NOCOSYM) to MC and FA. LL, FI, JME and FA are researchers of
497 CONICET; MM, JMP, CFF and JRM are fellows of the same institution.
498

499 **Author contributions**

500 MM, JMP, LL, CFF, JRM, NM, AC, MB and FA performed the experiments. JB, MB, FI, MC, JE and FA ana-
501 lyzed the data. JE and FA conceived the project. FA, JE and CFF wrote the manuscript with the contribu-
502 tion of all authors.
503

504 **References**

505 **Ariel, F., Jegu, T., Latrasse, D., Romero-Barrios, N., Christ, A., Benhamed, M., and Crespi, M.** (2014).
506 Noncoding transcription by alternative rna polymerases dynamically regulates an auxin-driven
507 chromatin loop. *Mol. Cell* **55**:383–396.

508 **Ariel, F., Romero-Barrios, N., Jégu, T., Benhamed, M., and Crespi, M.** (2015). Battles and hijacks:
509 Noncoding transcription in plants. *Trends Plant Sci.* **20**:362–371.

510 **Ariel, F., Lucero, L., Christ, A., Mammarella, M. F., Jegu, T., Veluchamy, A., Mariappan, K., Latrasse, D.,**
511 **Blein, T., Liu, C., et al.** (2020). R-Loop Mediated trans Action of the APOLO Long Noncoding RNA.
512 *Mol. Cell* **77**:1055-1065.e4.

513 **Balcerowicz, D., Schoenaers, S., and Vissenberg, K.** (2015). Cell Fate Determination and the Switch from
514 Diffuse Growth to Planar Polarity in Arabidopsis Root Epidermal Cells. *Front. Plant Sci.* **6**:1–13.

515 **Bardou, F., Ariel, F., Simpson, C. G., Romero-Barrios, N., Laporte, P., Balzergue, S., Brown, J. W. S., and**
516 **Crespi, M.** (2014). Long Noncoding RNA Modulates Alternative Splicing Regulators in Arabidopsis.
517 *Dev. Cell* **30**:166–176.

518 **Beyrne, C. C., Iusem, N. D., and González, R. M.** (2019). Effect of salt stress on cytosine methylation
519 within GL2, an Arabidopsis thaliana gene involved in root epidermal cell differentiation. Absence of
520 inheritance in the unstressed progeny. *Int. J. Mol. Sci.* **20**:1–13.

521 **Bhosale, R., Giri, J., Pandey, B. K., Giehl, R. F. H., Hartmann, A., Traini, R., Truskina, J., Leftley, N.,**
522 **Hanlon, M., Swarup, K., et al.** (2018). A mechanistic framework for auxin dependent Arabidopsis
523 root hair elongation to low external phosphate. *Nat. Commun.* **9**:1–9.

524 **Bruex, A., Kainkaryam, R. M., Wieckowski, Y., Kang, Y. H., Bernhardt, C., Xia, Y., Zheng, X., Wang, J. Y.,**
525 **Lee, M. M., Benfey, P., et al.** (2012). A Gene Regulatory Network for Root Epidermis Cell
526 Differentiation in Arabidopsis. *PLoS Genet.* **8**:1–20.
527 **Buah, J. N., Kawamitsu, Y., Sato, S., and Murayama, S.** (1999). Effects of Different Types and
528 Concentrations of Gelling Agents on the Physical and Chemical Properties of Media and the Growth
529 of Banana (Musa spp.) in Vitro. *Plant Prod. Sci.* **2**:138–145.
530 **Chen, Y. F., Li, L. Q., Xu, Q., Kong, Y. H., Wang, H., and Wu, W. H.** (2009). The WRKY6 transcription factor
531 modulates PHOSPHATE1 expression in response to low pi stress in arabidopsis. *Plant Cell* **21**:3554–
532 3566.
533 **Chu, C., Quinn, J., and Chang, H. Y.** (2012). Chromatin isolation by RNA purification (ChIRP). *J. Vis. Exp.*
534 Advance Access published March 25, 2012, doi:10.3791/3912.
535 **Clough, S. J., and Bent, A. F.** (1998). Floral dip: a simplified method for Agrobacterium-mediated
536 transformation of Arabidopsis thaliana. *Plant J.* **16**:735–43.
537 **Costa, S., and Shaw, P.** (2006). Chromatin organization and cell fate switch respond to positional
538 information in Arabidopsis. *Nature* **439**:493–496.
539 **Datta, S., Prescott, H., and Dolan, L.** (2015). Intensity of a pulse of RSL4 transcription factor synthesis
540 determines Arabidopsis root hair cell size. *Nat. Plants* **1**:1–6.
541 **Devaiah, B. N., Karthikeyan, A. S., and Raghothama, K. G.** (2007). WRKY75 transcription factor is a
542 modulator of phosphate acquisition and root development in Arabidopsis. *Plant Physiol.* **143**:1789–
543 1801.
544 **Dong, J., Chen, C., and Chen, Z.** (2003). Expression profiles of the Arabidopsis WRKY gene superfamily
545 during plant defense response. *Plant Mol. Biol.* **51**:21–37.
546 **Franco-Zorrilla, J. M., Valli, A., Todesco, M., Mateos, I., Puga, M. I., Rubio-Somoza, I., Leyva, A., Weigel,**
547 **D., García, J. A., and Paz-Ares, J.** (2007). Target mimicry provides a new mechanism for regulation
548 of microRNA activity. *Nat. Genet.* **39**:1033–1037.
549 **Friml, J., Yang, X., Michniewicz, M., Weijers, D., Quint, A., Tietz, O., Benjamins, R., Ouwerkerk, P. B. F.,**
550 **Ljung, K., Sandberg, G., et al.** (2004). A PINOID-dependent binary switch in apical-basal PIN polar
551 targeting directs auxin efflux. *Science* **306**:862–5.
552 **Ghashghaie, J., Brenckmann, F., and Saugier, B.** (1991). Effects of agar concentration on water status
553 and growth of rose plants cultured in vitro. *Physiol. Plant.* **82**:73–78.
554 **Guimil, S., and Dunand, C.** (2006). Patterning of Arabidopsis epidermal cells: epigenetic factors regulate
555 the complex epidermal cell fate pathway. *Trends Plant Sci.* **11**:601–609.

556 **Gyula, P., Baksa, I., Tóth, T., Mohorianu, I., Dalmay, T., and Szittya, G.** (2018). Ambient temperature
557 regulates the expression of a small set of sRNAs influencing plant development through NF-YA2 and
558 YUC2. *Plant Cell Environ.* **41**:2404–2417.
559 **Heo, J. B., and Sung, S.** (2011). Vernalization-mediated epigenetic silencing by a long intronic noncoding
560 RNA. *Science (80-.).* **331**:76–9.
561 **Hung, T., Wang, Y., Lin, M. F., Koegel, A. K., Kotake, Y., Grant, G. D., Horlings, H. M., Shah, N.,**
562 **Umbricht, C., Wang, P., et al.** (2011). Extensive and coordinated transcription of noncoding RNAs
563 within cell-cycle promoters. In *Nature Genetics*, pp. 621–629. NIH Public Access.
564 **Hwang, Y., Choi, H. S., Cho, H. M., and Cho, H. T.** (2017). Tracheophytes contain conserved orthologs of
565 a basic helix-loop-helix transcription factor that modulate ROOT HAIR SPECIFIC genes. *Plant Cell*
566 **29**:39–53.
567 **Ikeuchi, M., Iwase, A., Rymen, B., Harashima, H., Shibata, M., Ohnuma, M., Breuer, C., Morao, A. K., De**
568 **Lucas, M., De Veylder, L., et al.** (2015). PRC2 represses dedifferentiation of mature somatic cells in
569 Arabidopsis. *Nat. Plants* **1**:1–7.
570 **Jabnoune, M., Secco, D., Lecampion, C., Robaglia, C., Shu, Q., and Poirier, Y.** (2013). A Rice cis-Natural
571 antisense RNA acts as a translational enhancer for its cognate mRNA and contributes to phosphate
572 homeostasis and plant fitness. *Plant Cell* **25**:4166–4182.
573 **Jiang, H., Li, T., Qu, Y., Wang, X., Li, B., Song, J., Sun, X., Tang, Y., Wan, J., Yu, Y., et al.** (2018). Long non-
574 coding RNA SNHG15 interacts with and stabilizes transcription factor Slug and promotes colon
575 cancer progression. *Cancer Lett.* **425**:78–87.
576 **Jones, A. R., Kramer, E. M., Knox, K., Swarup, R., Bennett, M. J., Lazarus, C. M., Leyser, H. M. O., and**
577 **Grierson, C. S.** (2009). Auxin transport through non-hair cells sustains root-hair development. *Nat.*
578 *Cell Biol.* **11**:78–84.
579 **Karas, B., Amyot, L., Johansen, C., Sato, S., Tabata, S., Kawaguchi, M., and Szczyglowski, K.** (2009).
580 Conservation of Lotus and Arabidopsis basic helix-loop-helix proteins reveals new players in root
581 hair development. *Plant Physiol.* **151**:1175–1185.
582 **Kim, D. H., and Sung, S.** (2017). Vernalization-Triggered Intragenic Chromatin Loop Formation by Long
583 Noncoding RNAs. *Dev. Cell* **40**:302-312.e4.
584 **Kindgren, P., Ard, R., Ivanov, M., and Marquardt, S.** (2018). Transcriptional read-through of the long
585 non-coding RNA SVALKA governs plant cold acclimation. *Nat. Commun.* **9**:1–11.
586 **Kotake, Y., Kitagawa, K., Ohhata, T., Sakai, S., Uchida, C., Niida, H., Naemura, M., and Kitagawa, M.**
587 (2016). Long Non-coding RNA, PANDA, Contributes to the Stabilization of p53 Tumor Suppressor

588 Protein. *Anticancer Res.* **36**:1605–11.
589 **Lamport, D. T. A., Kieliszewski, M. J., Chen, Y., and Cannon, M. C.** (2011). Role of the Extensin
590 Superfamily in Primary Cell Wall Architecture. *Plant Physiol.* **156**:11–19.
591 **Lin, Q., Ohashi, Y., Kato, M., Tsuge, T., Gu, H., Qu, L. J., and Aoyama, T.** (2015). GLABRA2 directly
592 suppresses basic helix-loop-helix transcription factor genes with diverse functions in root hair
593 development. *Plant Cell* **27**:2894–2906.
594 **Liu, C., Wang, C., Wang, G., Becker, C., Zaidem, M., and Weigel, D.** (2016). Genome-wide analysis of
595 chromatin packing in Arabidopsis thaliana at single-gene resolution. *Genome Res.* **26**:1057–1068.
596 **Lucero, L., Fonouni-Farde, C., Crespi, M., and Ariel, F.** (2020). Long noncoding RNAs shape transcription
597 in plants. *Transcription* Advance Access published May 14, 2020,
598 doi:10.1080/21541264.2020.1764312.
599 **Mangano, S., Denita-Juarez, S. P., Choi, H. S., Marzol, E., Hwang, Y., Ranocha, P., Velasquez, S. M.,**
600 **Borassi, C., Barberini, M. L., Aptekmann, A. A., et al.** (2017). Molecular link between auxin and
601 ROS-mediated polar growth. *Proc. Natl. Acad. Sci. U. S. A.* **114**:5289–5294.
602 **Mangano, S., Martínez Pacheco, J., Marino-Buslje, C., and Estevez, J. M.** (2018a). How Does pH Fit in
603 with Oscillating Polar Growth? *Trends Plant Sci.* **23**:479–489.
604 **Mangano, S., Denita-Juarez, S. P., Marzol, E., Borassi, C., and Estevez, J. M.** (2018b). High Auxin and
605 High Phosphate Impact on RSL2 Expression and ROS-Homeostasis Linked to Root Hair Growth in
606 Arabidopsis thaliana. *Front. Plant Sci.* **9**:1–8.
607 **Marquardt, S., Raitskin, O., Wu, Z., Liu, F., Sun, Q., and Dean, C.** (2014). Functional Consequences of
608 Splicing of the Antisense Transcript COOLAIR on FLC Transcription. *Mol. Cell* **54**:156–165.
609 **Martianov, I., Ramadass, A., Serra Barros, A., Chow, N., and Akoulitchev, A.** (2007). Repression of the
610 human dihydrofolate reductase gene by a non-coding interfering transcript. *Nature* **445**:666–670.
611 **Marzol, E., Borassi, C., Denita Juárez, S. P., Mangano, S., and Estevez, J. M.** (2017). RSL4 Takes Control:
612 Multiple Signals, One Transcription Factor. *Trends Plant Sci.* **22**:553–555.
613 **Marzol, E., Borassi, C., Bringas, M., Sede, A., Rodríguez Garcia, D. R., Capece, L., and Estevez, J. M.**
614 (2018). Filling the Gaps to Solve the Extensin Puzzle. *Mol. Plant* **11**:645–658.
615 **Menand, B., Yi, K., Jouannic, S., Hoffmann, L., Ryan, E., Linstead, P., Schaefer, D. G., and Dolan, L.**
616 (2007). An ancient mechanism controls the development of cells with a rooting function in land
617 plants. *Science (80-.).* **316**:1477–1480.
618 **Nonami, H., and Boyer, J. S.** (1989). Turgor and Growth at Low Water Potentials. *Plant Physiol.* **89**:798–
619 804.

620 **Pires, N. D., Yi, K., Breuninger, H., Catarino, B., Menand, B., and Dolan, L.** (2013). Recruitment and
621 remodeling of an ancient gene regulatory network during land plant evolution. *Proc. Natl. Acad. Sci.*
622 *U. S. A.* **110**:9571–9576.
623 **Puvvula, P. K., Desetty, R. D., Pineau, P., Marchio, A., Moon, A., Dejean, A., and Bischof, O.** (2014). Long
624 noncoding RNA PANDA and scaffold-attachment-factor SAFA control senescence entry and exit.
625 *Nat. Commun.* **5**:1–16.
626 **Rigo, R., Bazin, J., Romero-Barrios, N., Moison, M., Lucero, L., Christ, A., Benhamed, M., Blein, T.,**
627 **Huguet, S., Charon, C., et al.** (2020). *An Arabidopsis long noncoding RNA modulates the*
628 *transcriptome through interactions with a network of splicing factors*. Cold Spring Harbor
629 Laboratory.
630 **Ringli, C.** (2010). The hydroxyproline-rich glycoprotein domain of the Arabidopsis LRX1 requires Tyr for
631 function but not for insolubilization in the cell wall. *Plant J.* **63**:662–669.
632 **Ryu, K. H., Kang, Y. H., Park, Y. H., Hwang, I., Schiefelbein, J., and Lee, M. M.** (2005). The WEREWOLF
633 MYB protein directly regulates CAPRICE transcription during cell fate specification in the
634 Arabidopsis root epidermis. *Development* **132**:4765–4775.
635 **Schiefelbein, J., Huang, L., and Zheng, X.** (2014). Regulation of epidermal cell fate in Arabidopsis roots:
636 the importance of multiple feedback loops. *Front. Plant Sci.* **5**:1–4.
637 **Schindelin, J., Arganda-Carreras, I., Frise, E., Kaynig, V., Longair, M., Pietzsch, T., Preibisch, S., Rueden,**
638 **C., Saalfeld, S., Schmid, B., et al.** (2012). Fiji: an open-source platform for biological-image analysis.
639 *Nat. Methods* **9**:676–682.
640 **Schoenaers, S., Balcerowicz, D., Breen, G., Hill, K., Zdanio, M., Mouille, G., Holman, T. J., Oh, J., Wilson,**
641 **M. H., Nikonorova, N., et al.** (2018). The Auxin-Regulated CrRLK1L Kinase ERULUS Controls Cell
642 Wall Composition during Root Hair Tip Growth. *Curr. Biol.* **28**:722-732.e6.
643 **Shi, W., Wang, Q., Bian, Y., Fan, Y., Zhou, Y., Feng, T., Li, Z., and Cao, X.** (2019). Long noncoding RNA
644 PANDA promotes esophageal squamous carcinoma cell progress by dissociating from NF-YA but
645 interact with SAFA. *Pathol. Res. Pract.* **215**:1–11.
646 **Singha, S., Townsend, E.C. and Oberly, G. H.** (1985). Mineral nutrient status of crabapple and pear
647 shoots cultured in vitro on varying commercial agars. *J. Am. Soc. Hortic. Sci.* **110**:407-411.
648 **Song, S. K., Ryu, K. H., Kang, Y. H., Song, J. H., Cho, Y. H., Yoo, S. D., Schiefelbein, J., and Lee, M. M.**
649 (2011). Cell fate in the Arabidopsis root epidermis is determined by competition between
650 WEREWOLF and CAPRICE. *Plant Physiol.* **157**:1196–1208.
651 **Sorenson, R., and Bailey-Serres, J.** (2015). Rapid immunopurification of ribonucleoprotein complexes of

652 plants. *Methods Mol. Biol.* **1284**:209–219.
653 **Stepanova, A. N., Robertson-Hoyt, J., Yun, J., Benavente, L. M., Xie, D. Y., Doležal, K., Schlereth, A.,**
654 **Jürgens, G., and Alonso, J. M.** (2008). TAA1-Mediated Auxin Biosynthesis Is Essential for Hormone
655 Crosstalk and Plant Development. *Cell* **133**:177–191.
656 **Su, T., Xu, Q., Zhang, F. C., Chen, Y., Li, L. Q., Wu, W. H., and Chen, Y. F.** (2015). WRKY42 Modulates
657 phosphate homeostasis through regulating phosphate translocation and acquisition in Arabidopsis.
658 *Plant Physiol.* **167**:1579–1591.
659 **Velasquez, S. M., Ricardi, M. M., Dorosz, J. G., Fernandez, P. V., Nadra, A. D., Pol-Fachin, L., Egelund, J.,**
660 **Gille, S., Harholt, J., Ciancia, M., et al.** (2011). O-glycosylated cell wall proteins are essential in root
661 hair growth. *Science (80-.).* **332**:1401–1403.
662 **Velasquez, S. M., Marzol, E., Borassi, C., Pol-Fachin, L., Ricardi, M. M., Mangano, S., Juarez, S. P. D.,**
663 **Salter, J. D. S., Dorosz, J. G., Marcus, S. E., et al.** (2015). Low Sugar Is Not Always Good: Impact of
664 Specific O -Glycan Defects on Tip Growth in Arabidopsis. *Plant Physiol.* **168**:808–813.
665 **Veluchamy, A., Jégu, T., Ariel, F., Latrasse, D., Mariappan, K. G., Kim, S.-K., Crespi, M., Hirt, H.,**
666 **Bergounioux, C., Raynaud, C., et al.** (2016). LHP1 Regulates H3K27me3 Spreading and Shapes the
667 Three-Dimensional Conformation of the Arabidopsis Genome. *PLoS One* **11**:1–25.
668 **Vijayakumar, P., Datta, S., and Dolan, L.** (2016). ROOT HAIR DEFECTIVE SIX-LIKE4 (RSL4) promotes root
669 hair elongation by transcriptionally regulating the expression of genes required for cell growth.
670 *New Phytol.* **212**:944–953.
671 **Waese, J., Fan, J., Pasha, A., Yu, H., Fucile, G., Shi, R., Cumming, M., Kelley, L. A., Sternberg, M. J.,**
672 **Krishnakumar, V., et al.** (2017). ePlant: Visualizing and exploring multiple levels of data for
673 hypothesis generation in plant biology. *Plant Cell* **29**:1806–1821.
674 **Wang, H., Xu, Q., Kong, Y. H., Chen, Y., Duan, J. Y., Wu, W. H., and Chen, Y. F.** (2014). Arabidopsis
675 WRKY45 transcription factor activates Phosphate transporter1;1 expression in response to
676 phosphate starvation. *Plant Physiol.* **164**:2020–2029.
677 **Wang, Q., Qin, G., Cao, M., Chen, R., He, Y., Yang, L., Zeng, Z., Yu, Y., Gu, Y., Xing, W., et al.** (2020). A
678 phosphorylation-based switch controls TAA1-mediated auxin biosynthesis in plants. *Nat. Commun.*
679 **11**:1–10.
680 **Won, S. K., Lee, Y. J., Lee, H. Y., Heo, Y. K., Cho, M., and Cho, H. T.** (2009). cis-element- and
681 transcriptome-based screening of root hair-specific genes and their functional characterization in
682 Arabidopsis. *Plant Physiol.* **150**:1459–1473.
683 **Xu, W., Li, K., Li, S., Hou, Q., Zhang, Y., Liu, K., and Sun, Q.** (2020). The R-Loop Atlas of Arabidopsis

684 Development and Responses to Environmental Stimuli. *Plant Cell* **32**:888–903.
685 **Yi, K., Menand, B., Bell, E., and Dolan, L.** (2010). A basic helix-loop-helix transcription factor controls cell
686 growth and size in root hairs. *Nat. Genet.* **42**:264–267.
687 **Zhang, T. Q., Xu, Z. G., Shang, G. D., and Wang, J. W.** (2019). A Single-Cell RNA Sequencing Profiles the
688 Developmental Landscape of Arabidopsis Root. *Mol. Plant* **12**:648–660.
689 **Zhang, Y., Chen, M., Siemiatkowska, B., Toleco, M. R., Jing, Y., Strotmann, V., Zhang, J., Stahl, Y., and**
690 **Fernie, A. R.** (2020). A Highly Efficient Agrobacterium-Mediated Method for Transient Gene
691 Expression and Functional Studies in Multiple Plant Species. *Plant Commun.* **1**:100028.
692

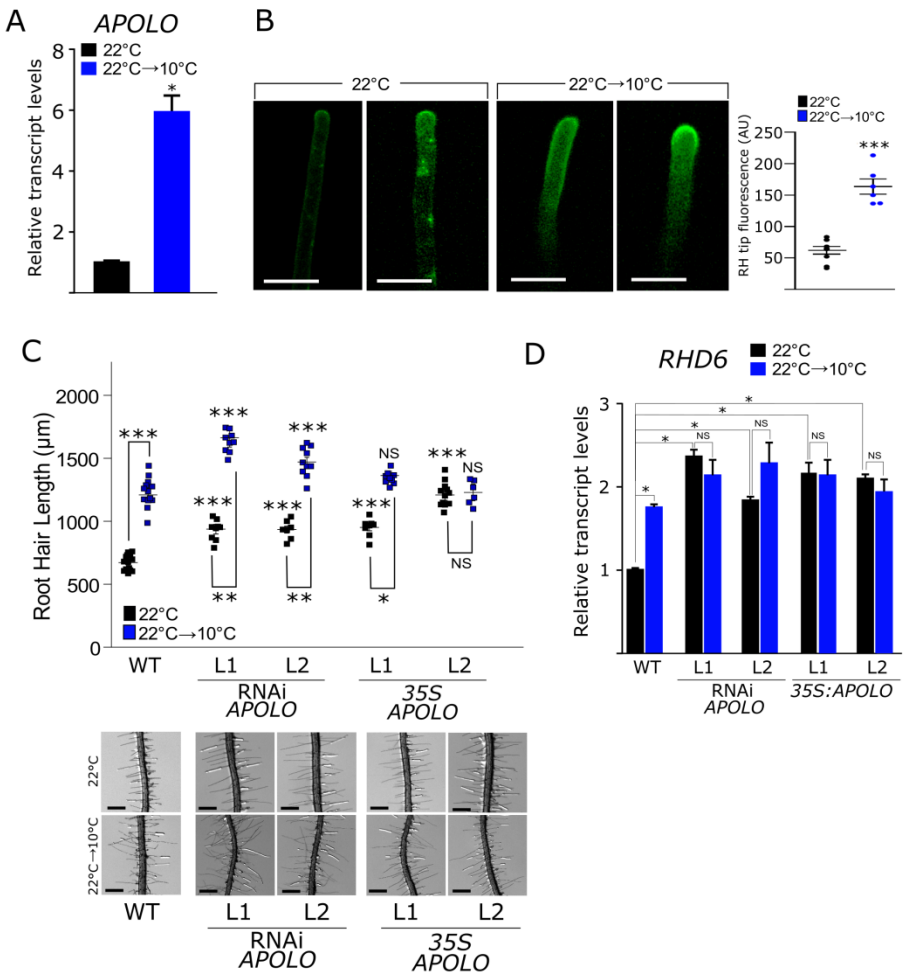

Figure 1. *APOLO* regulates root hair elongation in response to low temperatures

A. *APOLO* transcript levels measured by RT-qPCR in roots of 10-day-old plants grown at 22 °C treated or not for 24h at 10 °C.

B. The *APOLO* promoter region (full intergenic region between *PID* and *APOLO*) is active in root hairs at 22 °C and 10 °C, using the *GFP* reporter gene. Images are representative of the lowest and highest GFP signal detected in the observation of several roots. The quantification of the fluorescence is shown in the right panel.

C. Quantification of RH length of 8-day-old WT, RNAi-*APOLO* and *35S:APOLO* plants, respectively, at 22 °C and 10 °C. Each point is the mean ±error of the length of the 10 longest RHs identified in the root elongation zone in a single root. Representative images of each genotype are shown below the graph. The scale bas represent 500µm. Asterisks indicate significant differences between WT and the corresponding genotype at the same temperature or significant differences between temperature treatments on the same genotype at the same temperature (one way ANOVA followed by a Tukey-Kramer test; "*"<0.05, "**"<0.01, "***"<0.001). NS stands for no statistically significant difference.

D. *RHD6* transcript levels measured by RT-qPCR in roots of WT plants vs. two independent RNAi-*APOLO* lines and two independent *35S:APOLO* lines grown at 22 °C treated or not for 24h at 10 °C.

In A and D, the error bars represent the SD of 3 biological replicates. The asterisks indicate that the differences are significant (t test p<0.05). Values are normalized using the constant housekeeping transcript *PP2A*.

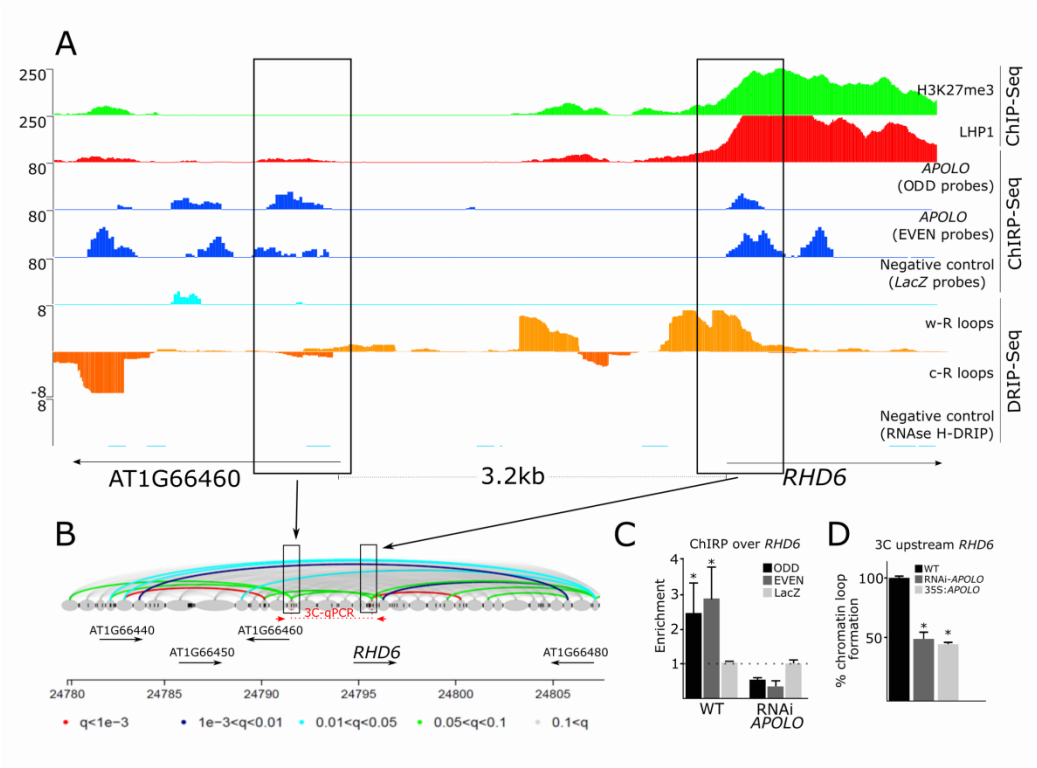

Figure 2. *APOLO* directly modulates chromatin three-dimensional conformation of the *RHD6* locus

A. Epigenomic landscape of the *RHD6* locus. Lane 1: H3K27me3 deposition by ChIP-Seq (Veluchamy et al., 2016). Lane 2: LHP1 deposition by ChIP-Seq (Veluchamy et al., 2016). Lane 3 to 5: *APOLO* recognition by ChIRP-Seq (Lane 3 and 4, using ODD and EVEN sets of probes against *APOLO*, respectively; Lane 5, negative control using LacZ probes)(Ariel et al., 2020). Lane 6 to 8: R-loop formation by DRIP-Seq (R-loop Atlas, root samples,(Xu et al., 2020), on Watson strand (Lane 6) and Crick strand (Lane 7). DRIP negative control after RNAseH treatment is shown in Lane 8. Gene annotation is shown at the bottom.

B. Chromatin loops identified in the *RHD6* region by *Dpn*II HiC (Liu et al., 2016). Colors of the loops are related to the corresponding q-values indicated below. Black boxes in A and B indicate the same genomic locations, where the bases of the chromatin loop correlate with R-loop formation and *APOLO* recognition (compared to gene annotations). In red the arrows indicate the position of the probes used for 3C-qPCR shown in **D**.

C. *APOLO* association to DNA of the *RHD6* locus by ChIRP-qPCR in WT and RNAi-*APOLO* plants. The background level was determined using a set of probes against LacZ RNA.

D. Relative chromatin loop formation by 3C-qPCR deduced from **B**, in WT plants vs. *35S:APOLO* and RNAi lines for the region upstream *RHD6*. The probes used for 3C-qPCR are indicated in red in panel **B**.

In C and D, the error bars represent the SD of 3 biological replicates. The asterisks indicate that the differences are significant (t test "*"<0.05, "***"<0.001).

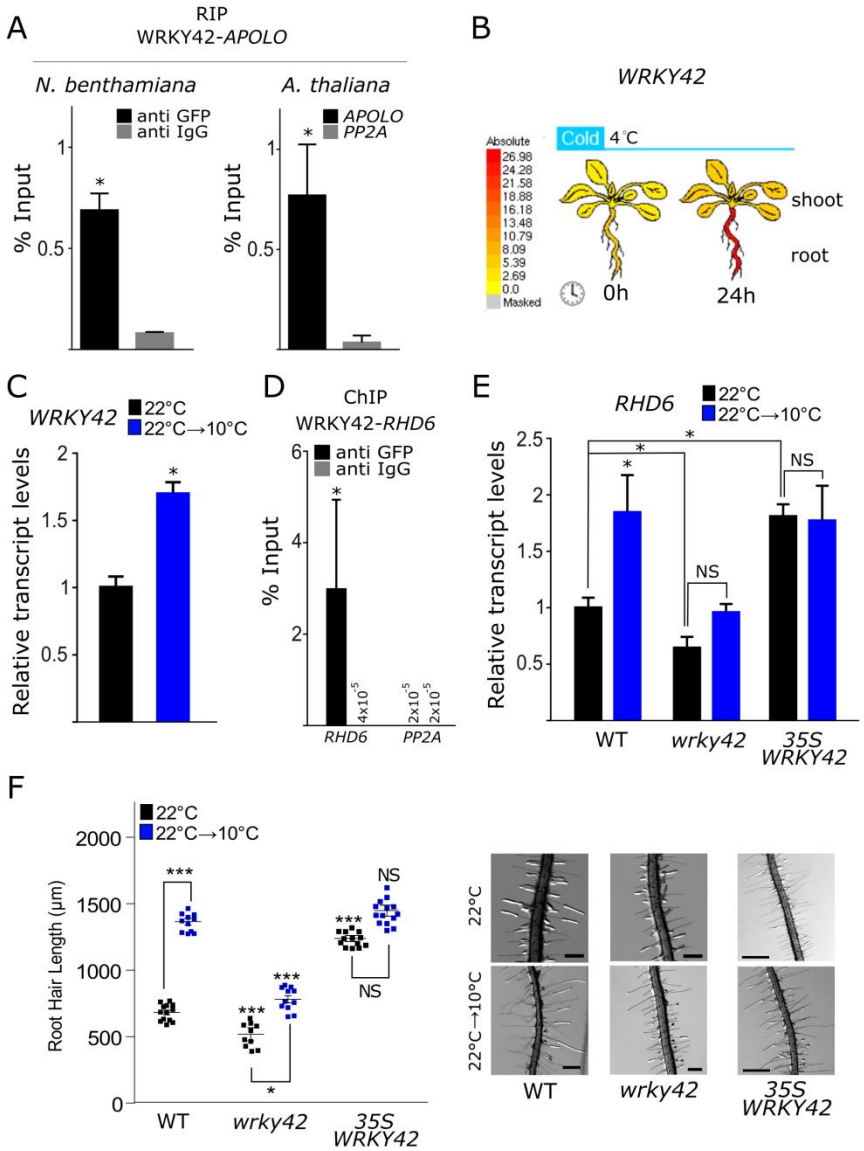

Figure 3. The transcription factor WRKY42 interacts with *APOLO*, directly regulates *RHD6* and participates in the response to cold

A. *APOLO*-WRKY42 *in vivo* interaction demonstrated by RNA Immunoprecipitation (RIP)-qPCR in transiently transformed tobacco leaves and stably transformed Arabidopsis plants. In tobacco, WRKY42:GFP and *APOLO* were co-transformed under the control of the 35S constitutive promoter. In Arabidopsis, *35S:WRKY42:GFP* transformed plants were used to detect the interaction with endogenous *APOLO*. Anti-IgG antibodies were used as a negative control. The RNA *PP2A* was considered as a RIP negative control in Arabidopsis plants.

B. Arabidopsis eFP Browser (Waese et al., 2017) plot representing the increase of *WRKY42* transcript levels in roots of seedlings treated for 24h at 4°C.

C. *WRKY42* transcript levels measured by RT-qPCR in roots of plants grown at 22°C treated or not for 24h at 10°C.

745 **D.** Chromatin Immunoprecipitation (ChIP)-qPCR assay revealing regulation by WRKY42 of *RHD6* by direct
746 recognition of its promoter region. Probes amplifying *PP2A* were used as a negative control of the exper-
747 iment. Anti-IgG antibodies were used as a negative control for each pair of probes.
748 **E.** *RHD6* transcript levels measured by RT-qPCR in roots of WT plants vs. *wrky42* mutants and
749 *35S:WRKY42:GFP* lines grown at 22°C treated or not for 24h at 10°C.
750 **F.** Quantification of RH length of WT, *wrky42* and *35S:WRKY42:GFP* plants at 22°C and 10°C. Each point is
751 the mean of the length of the 10 longest RHs identified in a single root. Representative images of each
752 genotype are shown on the right. The scale bas represent 500µm. Asterisks indicate significant differ-
753 ences between WT and the corresponding genotype at the same temperature (one way ANOVA followed
754 by a Tukey-Kramer test; "*"<0.05, "***"<0.001).
755 In A, C, D and E, the error bars represent the SD of 3 biological replicates. The asterisks indicate that the
756 differences are significant (t test p<0.05). NS stands for no statistically significant difference. In C and E,
757 values are normalized using the constant housekeeping transcript *PP2A*.

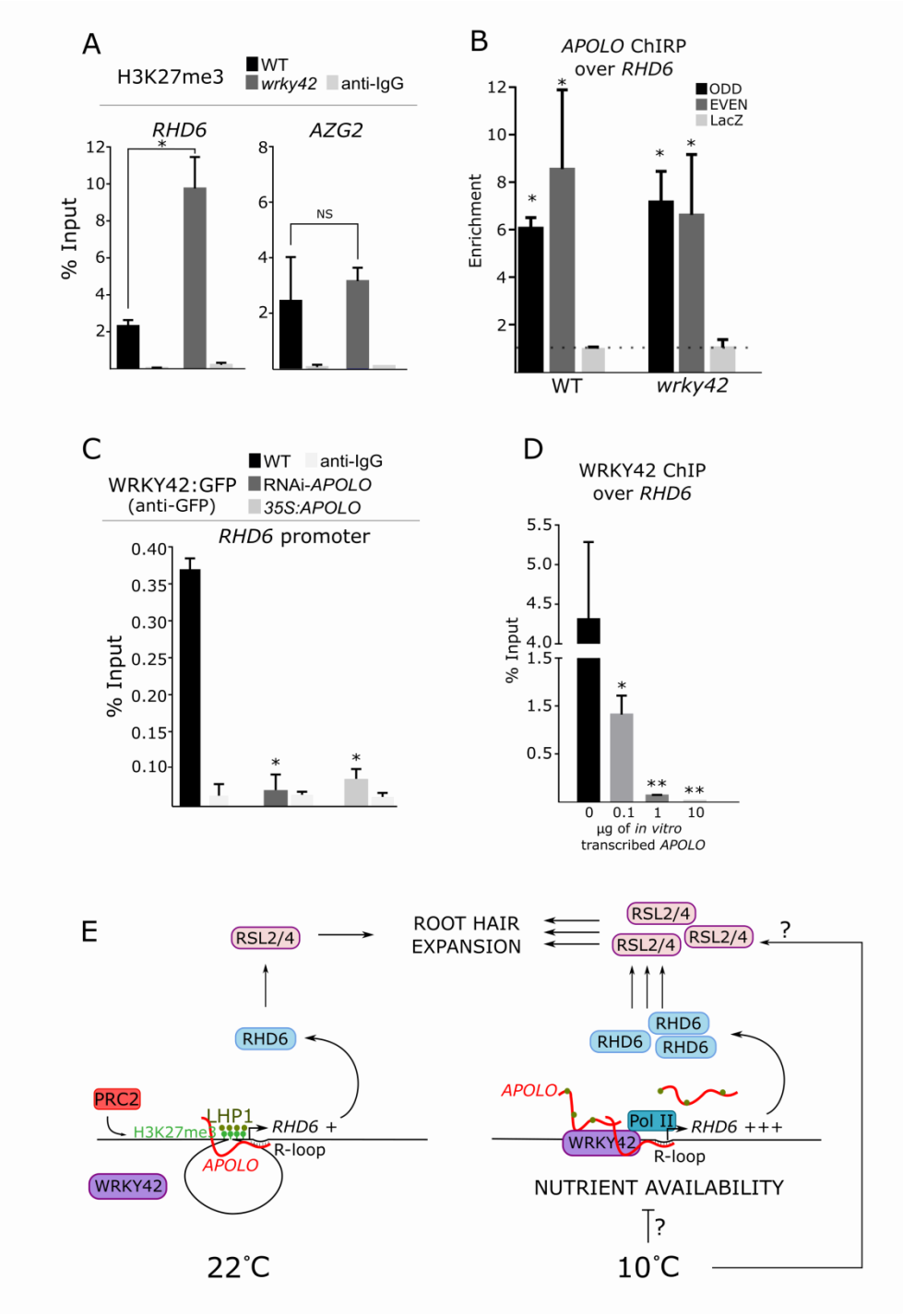

758

759 **Figure 4. The WRKY42-*APOLO* hub activates *RHD6* transcription in response to low temperatures, pro-**
760 **moting root hair expansion**
761 **A.** H3K27me3 deposition in WT vs. *wrky42* mutant 10-day-old seedlings grown at 23°C over *RHD6* and a
762 WRKY42-independent *APOLO* target (*AZG2*; (Ariel et al., 2020)). An immunoprecipitation (ChIP-qPCR) was
763 performed using an anti-IgG antibody as a negative control.
764 **B.** *APOLO* association to DNA of the *RHD6* locus by ChIRP-qPCR in WT and *wrky42* mutant plants. The
765 background level was determined using a set of probes against LacZ RNA.

766 **C.** WRKY42 binding to *RHD6* promoter in transiently transformed leaves of WT, RNAi-*APOLO* and
767 *35S:APOLO* plants. WRKY42:GFP was immunoprecipitated using the anti-GFP antibody (ChIP-qPCR). An
768 immunoprecipitation was performed using an anti-IgG antibody as a negative control.
769 **D.** WRKY42 immunoprecipitation over *RHD6* with the addition of increasing concentrations of *in vitro*
770 transcribed *APOLO* prior to cross-linking.
771 **E.** Proposed model for the action of *APOLO* in RH growth under low temperatures. At 22 °C, *RHD6* mod-
772 erate transcription is regulated by *APOLO*, H3K27me3 and LHP1, maintaining a repressive chromatin loop
773 encompassing the *RHD6* promoter region. In response to cold, *APOLO* levels increase, still recognizing the
774 *RHD6* locus by sequence complementarity (R-loops). Then, LHP1 (brown balls) is decoyed away from
775 chromatin and PRC2-dependent H3K27me3 (green balls) deposition decreases in a process involving
776 WRKY42 and leading to the opening of the *RHD6* promoter region. Additionally, *APOLO* and WRKY42
777 jointly activate *RHD6* transcription. RHD6 activates the transcription of downstream TF genes *RSL2* and *4*
778 promoting RH cell expansion. Yet unknown factors activate *RSL2* and *4* independently from *APOLO* and
779 RHD6 in response to cold.
780 In A to D the error bar represents the SD of 3 biological replicates. The asterisk indicates that the differ-
781 ence is significant (t test "*"<0.05, "**"<0.01).

782

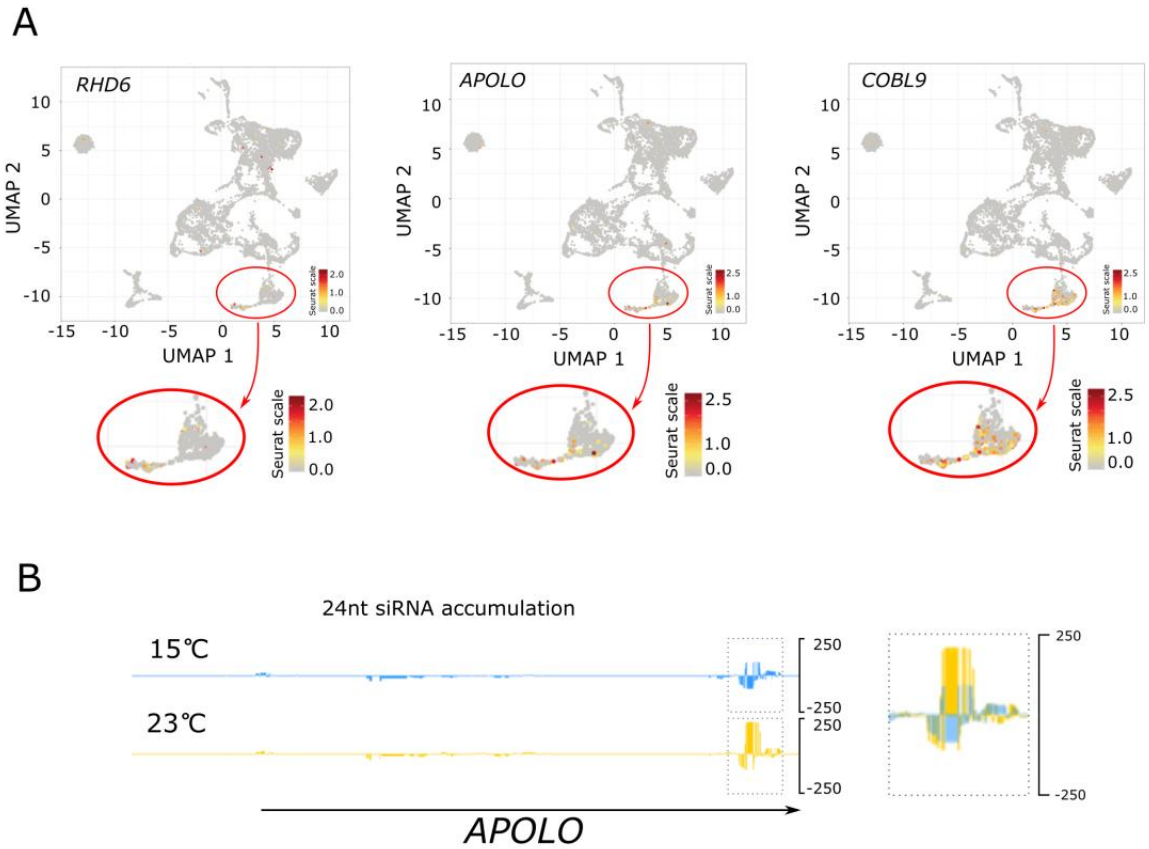

Supplementary Figure 1: *RHD6* and *APOLO* transcripts are enriched in root hair cells

A. Uniform Manifold Approximation and Projection (UMAP) clustering map of Arabidopsis root single cell RNA-seq ((Zhang et al., 2019); http://wanglab.sippe.ac.cn/rootatlas/) data. *RHD6*, *APOLO* and the trichoblast cell marker *COBL9* are respectively indicated in red in each plot.

B. 24nt siRNA accumulation over the *APOLO* locus revealed by small RNA-Seq of roots from WT seedlings grown at 15 °C or 23 °C (Gyula et al., 2018). On the right, a zoom of the 3' region is shown, with the overlapped signal at both temperatures.

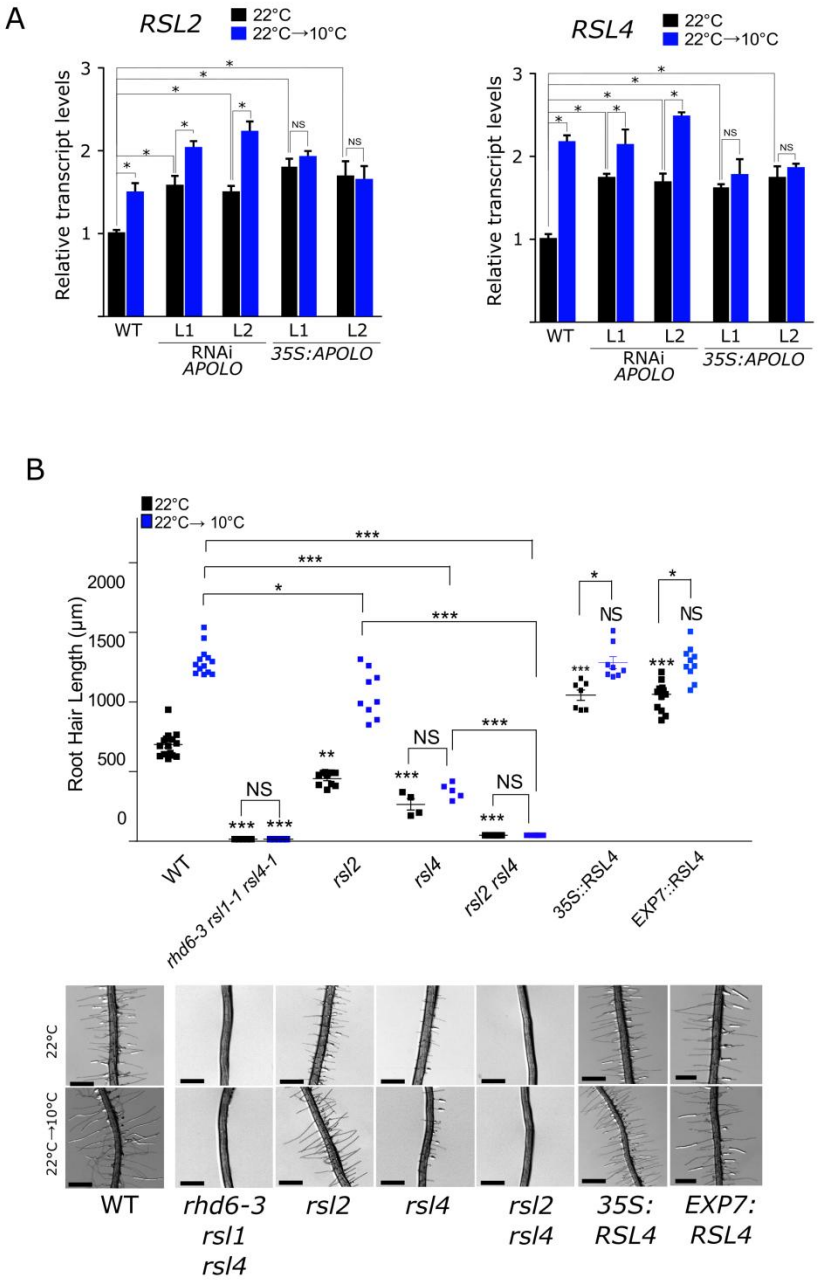

Supplementary Figure 2. Root hair expansion in response to cold is mediated by *RSL2* and *RSL4*

A. *RSL2* and *RSL4* transcript levels measured by RT-qPCR in roots of WT plants vs. two independent RNAi-*APOLO* lines and two independent *35S:APOLO* lines grown at 22 °C treated or not for 24h at 10 °C. The asterisks indicate that the differences are significant (t test $p<0.05$). NS stands for no statistically significant difference. Values are normalized using the constant housekeeping transcript *PP2A*.

B. Quantification of RH length of plants WT, *rhd6-3, rsl1/4; rsl2; rsl4; rsl2/4*; *35S:RSL4* and *pEXP7:RSL4* at 22°C and 10°C. Each point is the mean ±error of the length of the 10 longest RHs identified in the root elongation zone in a single root. Representative images of each genotype are shown below the graph. The scale bas represent 500µm. Asterisks indicate significant differences between WT and the corresponding genotype at the same temperature or significant differences between temperature treatments

802 on the same genotype at the same temperature (one way ANOVA followed by a Tukey-Kramer test;
803 “*”<0.05, “**”<0.01, “***”<0.001), unless indicated differently. NS stands for no statistically significant
804 difference.

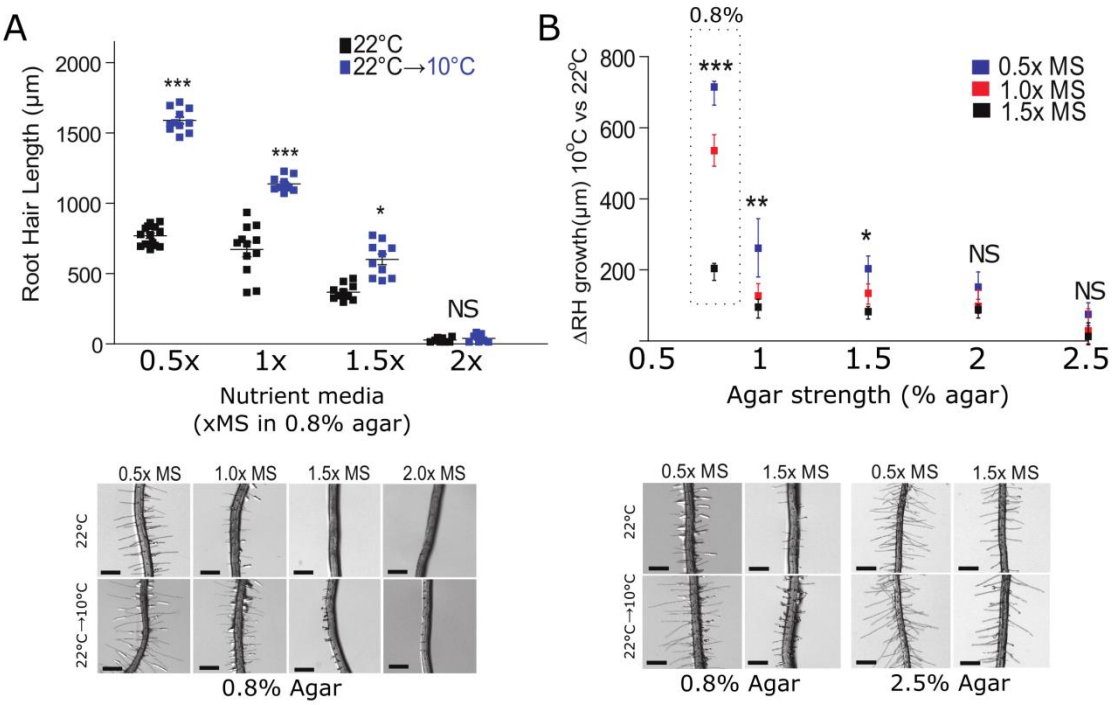

Supplementary Figure 3. Root hair expansion in response to cold seems to be related to nutrient availability

A. Quantification of RH length of WT plants at 22°C and 10°C at growing concentrations of Murashige and Skoog (MS) culture media. Each point is the mean ±error of the length of the 10 longest RHs identified in the root elongation zone in a single root. Representative images of each genotype are shown below. Asterisks indicate significant differences between temperature treatments on a specific nutrient media condition (one way ANOVA followed by a Tukey-Kramer test; "*"<0.05, "***"<0.001). NS stands for no statistically significant difference.

B. Quantification of RH length of WT plants expressed as the ratio between 10°C and 22°C at growing concentrations of MS culture media, for given concentrations of agar. Representative images of each genotype are shown below the graph. Each point is the mean ±error of the length of the 10 longest RHs identified in the root elongation zone in a single root. Note that at higher concentrations of agar, the ΔRH between conditions is lower, but the RHs are longer (as shown in the representative photos below). Asterisks indicate significant differences between agar percentage conditions (one way ANOVA followed by a Tukey-Kramer test; "*"<0.05, "**"<0.01, "***"<0.001). NS stands for no statistically significant difference. The dotted box indicates the same results as in panel A, expressed as ΔRH growth instead of absolute RH length at 22°C and 10°C independently. In the photos in A and B, the scale bas represent 500µm.

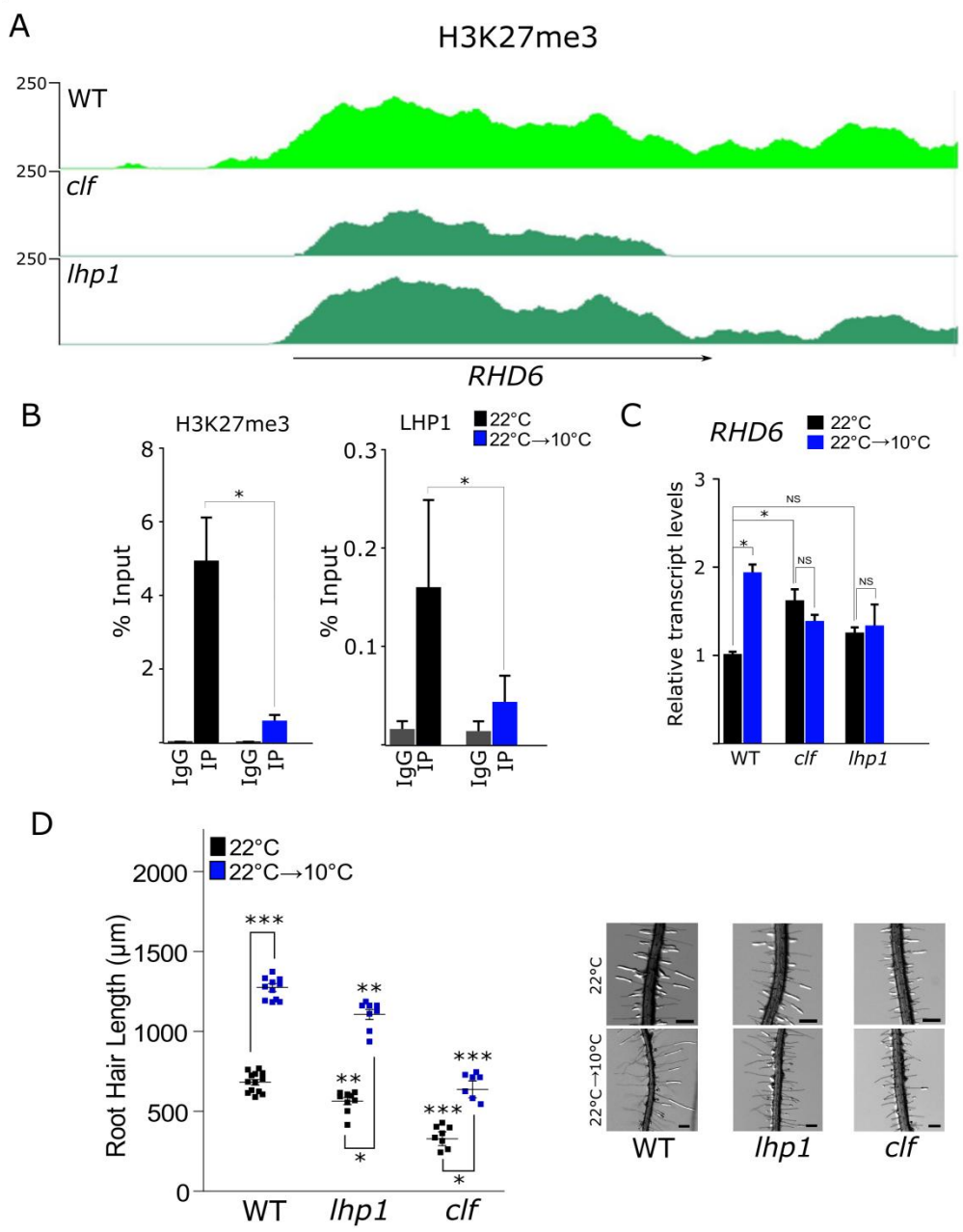

Supplementary Figure 4: Induction of root hair elongation by low temperatures requires epigenetic Polycomb-mediated reprogramming

A. H3K27me3 deposition across the *RHD6* locus in WT, *clf* and *lhp1* mutants, revealed by ChIP-seq from seedlings grown at 23°C (Veluchamy et al., 2016).

B. H3K27me3 deposition measured by ChIP-qPCR over the *RHD6* locus in WT plants grown at 22°C treated or not for 24h at 10°C. The negative control was performed using an anti-IgG antibody.

C. *RHD6* transcript levels measured by RT-qPCR in roots of WT plants vs. *clf* and *lhp1* mutants grown at 22 °C treated or not for 24h at 10 °C.

D. Quantification of RH length of plants WT, *lhp1* and *clf* at 22°C and 10°C. Each point is the mean ±error of the length of the 10 longest RHs identified in the root elongation zone in a single root. Representative

835 images of each genotype are shown on the right. The scale bas represent 500µm. Asterisks indicate sig-
836 nificant differences between WT and the corresponding genotype at the same temperature or significant
837 differences between temperature treatments on the same genotype at the same temperature (one way
838 ANOVA followed by a Tukey-Kramer test; “**”<0.01, “***”<0.001).
839 In B and C, the error bars represent the SD of 3 biological replicates. The asterisks indicate that the dif-
840 ference are significant (t test p<0.05).
841
842

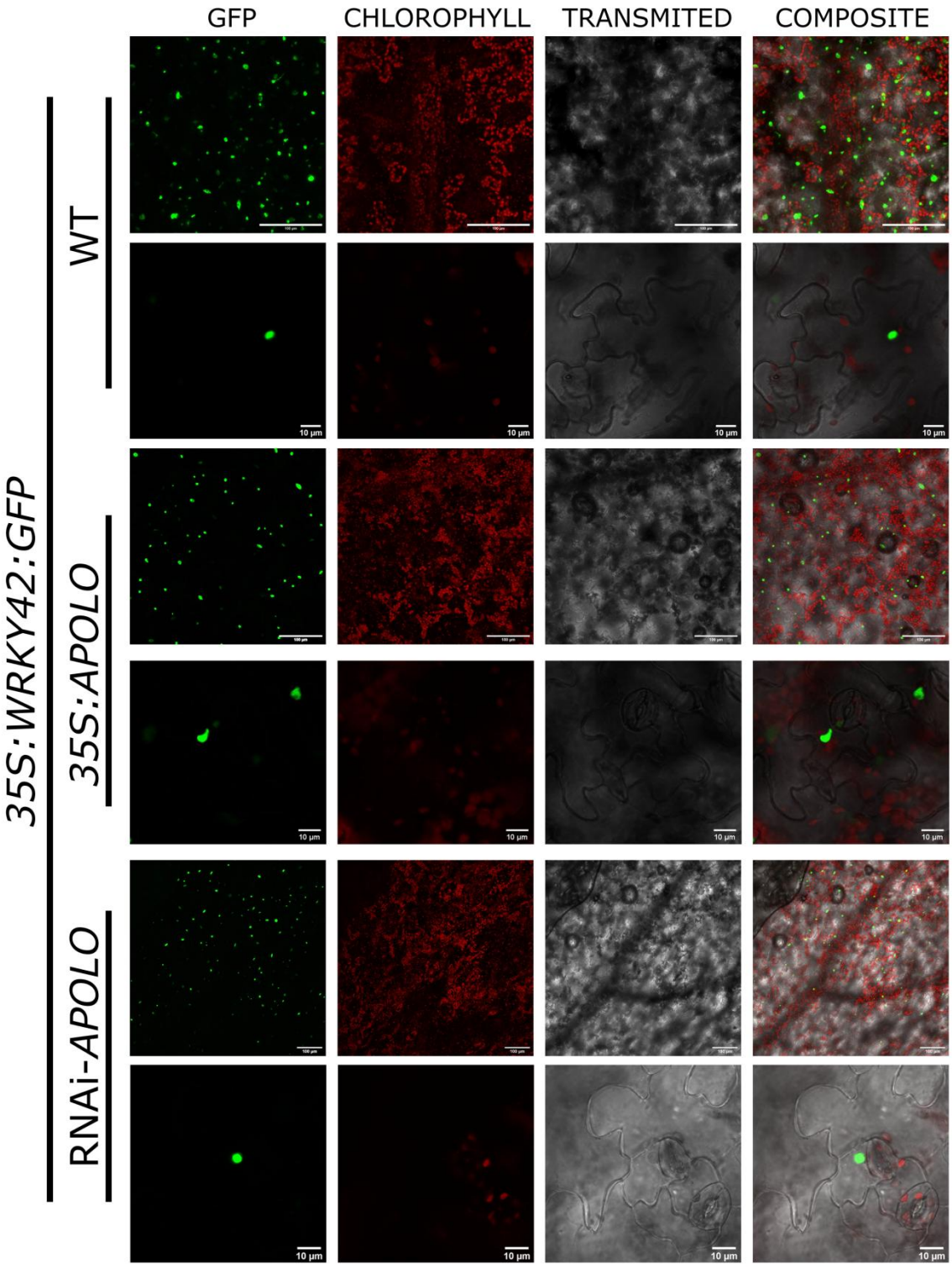

843
844
845 **Supplementary Figure 5: WRKY42:GFP is localized in the cell nucleus, regardless the expression levels**
846 **of *APOLO*.**
847 Confocal observation of the GFP tag of WRKY42, transiently expressed in leaves of WT, *35S:APOLO* and
848 RNAi-*APOLO* plants. Samples were excited at 488 nm (Intensity=8%) and detected at 495-530 nm for GFP

849 and 610-670 (gain 650) nm for chlorophyll fluorescence. Images were captured using 10X and 20X lenses
850 and the scale bars are indicated accordingly. The images show a high efficiency of leaf transformation for
851 every genetic background.

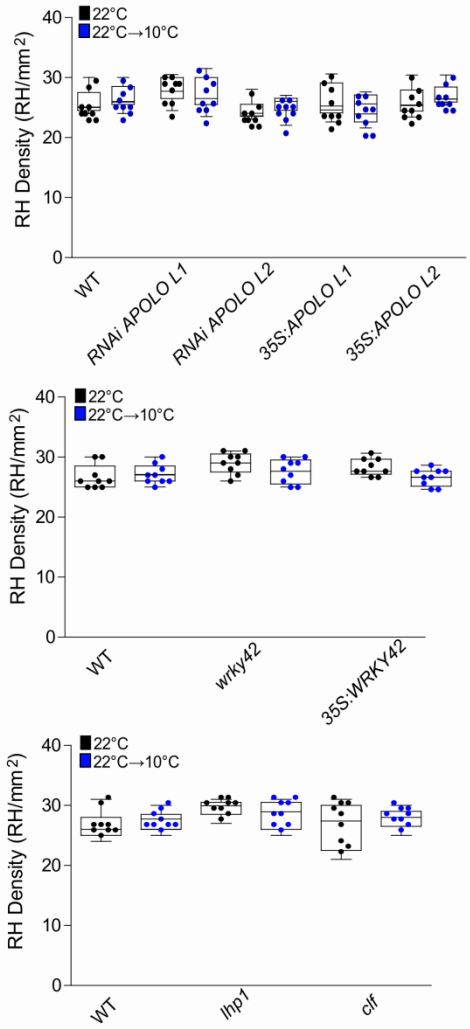

Supplementary Figure 6: Root hair density is not altered by the deregulation of *APOLO*, *WRKY42*, *LHP1* or *CLF*.

Root hair density was determined as described in the Materials and Methods section. All the lines used in this work exhibit a similar density (one way ANOVA followed by a Tukey-Kramer test; not significant) under control conditions as well as in response to cold treatment. Each point is the mean of the length of the 10 longest RHs identified in a single root.

861 **LEGENDS TO SUPPLEMENTARY TABLES**
862
863 **Supplementary Table 1: *APOLO* targets related to root hair growth.**
864 The list of *APOLO bona fide* targets was determined in (Ariel et al., 2020). The search for root hairs-
865 related genes was performed based on (Won et al., 2009; Yi et al., 2010; Vijayakumar et al., 2016; Hwang
866 et al., 2017). LHP1 binding and H3K27me3 deposition was investigated in previously published datasets
867 (Veluchamy et al., 2016). W-boxes (TTGACY;(Dong et al., 2003)) present in the first 2500 bp upstream
868 the ATG of each gene was searched manually. The position of box is given only for *RHD6*, directly recog-
869 nized by WRKY42 (**Figure 4C**).
870
871 **Supplementary Table 2: Root hair-related genes deregulated in *35S:APOLO* seedlings.**
872 The list of deregulated genes was determined by RNA-Seq (Ariel et al., 2020). The search for root hairs-
873 related genes was performed based on (Won et al., 2009; Yi et al., 2010; Vijayakumar et al., 2016; Hwang
874 et al., 2017). Genes are classified as directly (same as in **Supplementary Table 1**) or indirectly regulated
875 by *APOLO*. *RHD6*, *RSL2* and *RSL4* are highlighted in red.
876
877 **Supplementary Table 3: List of oligonucleotides used in this work.**